

# Amyloidogenicity of recombinant human pro-islet amyloid polypeptide (ProIAPP)

Monika Krampert<sup>1,2</sup>, Jürgen Bernhagen<sup>2</sup>, Jürgen Schmucker<sup>2</sup>, Anita Horn<sup>1</sup>, Anke Schmauder<sup>1</sup>, Herwig Brunner<sup>2</sup>, Wolfgang Voelter<sup>1</sup> and Aphrodite Kapurniotu<sup>1</sup>

**Background:** Pancreatic amyloid has been associated with type II diabetes. The major constituent of pancreatic amyloid is the 37-residue peptide islet amyloid polypeptide (IAPP). IAPP is expressed as a 67-residue pro-peptide called ProIAPP which is processed to IAPP following stimulation. While the molecular events underlying IAPP amyloid formation *in vitro* have been studied, little is known about the role of ProIAPP in the formation of pancreatic amyloid. This has been due in part to the limited availability of purified ProIAPP for conformational and biochemical studies.

**Results:** We present a method for efficient recombinant expression and purification of ProIAPP and a processing site mutant, mutProIAPP, as thioredoxin (Trx) fusion proteins. Conformation and amyloidogenicity of cleaved ProIAPP and mutProIAPP and the fusion proteins were assessed by circular dichroism, electron microscopy and Congo red staining. We find that ProIAPP and mutProIAPP exhibit strong self-association potentials and are capable of forming amyloid. However, the conformational transitions of ProIAPP and mutProIAPP during aging and amyloidogenesis are distinct from the random coil-to- $\beta$ -sheet transition of IAPP. Both proteins are found to be less amyloidogenic than IAPP and besides fibrils a number of non-fibrillar but ordered aggregates form during aging of ProIAPP. ProIAPP aggregates are cytotoxic on pancreatic cells but less cytotoxic than IAPP while mutProIAPP aggregates essentially lack cytotoxicity. The Trx fusion proteins are neither amyloidogenic nor cytotoxic.

**Conclusions:** Our studies suggest that ProIAPP has typical properties of an amyloidogenic polypeptide but also indicate that the pro-region suppresses the amyloidogenic and cytotoxic potentials of IAPP.

## Introduction

Pancreatic islet amyloid is found in more than 95% of type II diabetes patients and is believed to be associated with the pathologic sequelae of the disease [1–3]. Islet amyloid consists predominantly of insoluble aggregates that are derived from islet amyloid polypeptide (IAPP or amylin) [1,4]. IAPP is a 37-amino acid residue peptide that is mainly produced in pancreatic  $\beta$ -cells. Its soluble form plays a role in glucose homeostasis, possibly as an insulin counterregulatory hormone [5]. IAPP-derived amyloid aggregates, however, are strongly cytotoxic to a variety of cells, including  $\beta$ -cells [6,7].

IAPP is among the most amyloidogenic polypeptides known [8–13]. The molecular cause of IAPP fibrillization is not yet known. However, as to the *in vitro* mechanism of amyloidogenesis, it appears that IAPP follows kinetics that are consistent with the nucleation-dependent polymerization mechanism [12–14].

<sup>1</sup>Physiological-Chemical Institute, University of Tübingen, Hoppe-Seyler-Str. 4, D-72076 Tübingen, Germany

<sup>2</sup>Laboratory of Biochemistry, Institute for Interfacial Engineering, University of Stuttgart, Fraunhofer Institute FhIGB, D-70569 Stuttgart, Germany

Correspondence: Aphrodite Kapurniotu  
E-mail: afroditu.kapurniotu@uni-tuebingen.de

**Keywords:** Aggregation; Amyloidogenicity; Cytotoxicity; Islet amyloid polypeptide; Pro-islet amyloid polypeptide

Received: 25 April 2000

Revision requested: 5 June 2000

Revisions received: 5 September 2000

Accepted: 8 September 2000

Published: 21 September 2000

**Chemistry & Biology** 2000, 7:855–871

1074-5521/00/\$ – see front matter

© 2000 Elsevier Science Ltd. All rights reserved.

PII: S 1 0 7 4 - 5 5 2 1 ( 0 0 ) 0 0 0 3 4 - X

IAPP is expressed as an 89-amino acid precursor protein (preProIAPP). Cleavage of the N-terminal signal peptide yields ProIAPP, a 67-residue protein that contains the 37-amino acid IAPP sequence flanked by 11- and 19-amino acid N- and C-terminal pro-sequences, respectively [15] (Figure 1A). IAPP is derived from ProIAPP by post-translational processing in the secretory granules of pancreatic  $\beta$ -cells and is likely co-secreted with insulin into the circulation in response to insulin secretagogues [15].

The role of ProIAPP and its processing in the formation of pancreatic amyloid *in vivo* is poorly understood. Recent studies have suggested that ProIAPP is processed by the prohormone convertase PC2 which also is involved in the processing of proinsulin and that abnormal processing of ProIAPP may contribute to an IAPP-based amyloidosis [16]. If, for example, the rate of ProIAPP processing increased, higher concentrations of the strongly amyloidogenic IAPP would accumulate that could then lead to an

increase in amyloid deposit [17]. Conversely, if the rate of ProIAPP processing slowed down or was incomplete, increased amounts of ProIAPP would accumulate. The result of the latter scenario cannot be predicted currently, because it is not known if ProIAPP is amyloidogenic and cytotoxic per se. There have been no reports about the molecular and conformational properties of ProIAPP. This is due in part to the current lack of efficient procedures for a recombinant or synthetic generation of ProIAPP in amounts sufficient for such studies. There are a number of experimental difficulties expected to be encountered during ProIAPP generation. These are either pertinent to the chemical synthesis or recombinant expression and purification of amyloidogenic proteins or specific to the strong amyloidogenicity of IAPP [10,13,18,19].

We devised a method for the efficient recombinant expres-

sion of ProIAPP as thioredoxin (Trx) fusion protein in *Escherichia coli* in combination with a His-Tag-based and high performance liquid chromatography (HPLC) purification procedure. This method enables pure ProIAPP to be obtained for the first time in preparative amounts. In addition, a ProIAPP processing site mutant protein, mutProIAPP, with each of the two Lys-Arg proteinase cleavage sites of ProIAPP (Lys<sup>10</sup>-Arg<sup>11</sup> and Lys<sup>50</sup>-Arg<sup>51</sup> (Figure 1A)) substituted for Ala-Ala was designed and expressed using an identical approach. The substitutions were expected to render the mutProIAPP molecule resistant to processing in a bioassay setting. We subsequently performed studies on the solution conformation and putative amyloidogenic and cytotoxic potential of ProIAPP, mutProIAPP and their fusion constructs using a variety of biochemical methods including the Congo red (CR) staining method, electron microscopy (EM), circular di-

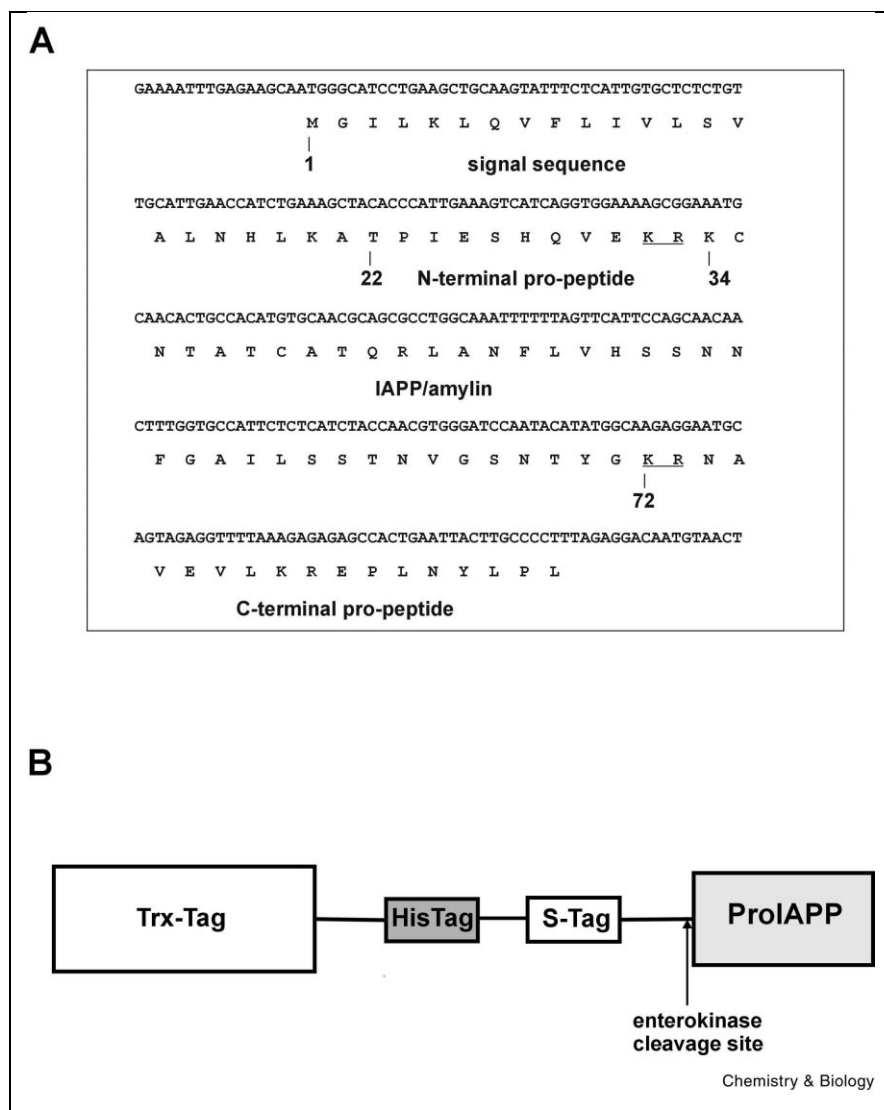


**Figure 1.** Schematic representation of the sequence and fusion construct of ProIAPP. **(A)** cDNA and amino acid sequence of preProIAPP, ProIAPP and IAPP. The signal sequence and the N- and C-terminal pro-regions are indicated. Upper lines represent nucleotides and lower lines are the corresponding amino acids. Numbers indicate the translational start site (1), the signal sequence cleavage site (22), and the N- (34) and C-terminal (72) pro-region cleavage sites. **(B)** Scheme of the fusion constructs expressed. The ProIAPP or mutProIAPP cDNA was fused C-terminally to the tag region of the vector. The Ek cleavage site for removal of the tag is indicated. The S-Tag was not utilized in this study. The fusion constructs have a size of about 24.5 kDa; the tag region corresponds to a size of 17 kDa; and ProIAPP or mutProIAPP are about 7.5 kDa in size.

chroism spectropolarimetry (CD), and a cellular toxicity assay.

## Results

### Design, expression, and purification of recombinant ProIAPP and mutProIAPP

We used the *E. coli* BL21(DE3)pLysS-pET vector over-expression system to produce ProIAPP and mutProIAPP. This system has previously been demonstrated to efficiently suppress unwanted expression activity of potentially toxic proteins [20]. Cloning strategies were designed for the expression of both ProIAPP alone and the Trx-ProIAPP fusion protein. Identical strategies were applied to mutProIAPP and the Trx-mutProIAPP fusion protein.

The testing of mutProIAPP was thought to provide information about the proteolytic stability of ProIAPP to the proinsulin- and proIAPP-processing endopeptidases when incubated with RIN5fm cells [16,21–23]. These enzymes might possibly process exogenously applied ProIAPP into IAPP during the 24-h incubation period of the cellular assay and following fibril/aggregate-mediated disruption of the cell membrane [24,25]. As the mutant protein would not be processed to IAPP, its application was predicted to be useful in distinguishing ProIAPP- from IAPP-mediated effects. However, we also noted that the Lys-Arg-to-Ala-Ala substitution resulted in a significant enhancement of hydrophobicity of both the N-terminal sequence up to residue Ala<sup>16</sup> and the C-terminal sequence (45–56) according to hydrophobicity analysis by the method of Kyte and Doolittle [26] (data not shown).

Trx has previously been used successfully as a fusion moiety to recombinantly express insoluble proteins in *E. coli* [27]. For convenient purification of the fusion protein, an additional His-Tag was included (Figure 1B). The fusion tag could be removed by enterokinase (Ek) cleavage close to the N-terminal Thr residue of the pro-sequence, resulting in wild type (wt) ProIAPP or mutProIAPP except for one additional N-terminal Ile residue. The fusion proteins Trx-ProIAPP and Trx-mutProIAPP were efficiently expressed when bacterial cultures were induced with 1 mM isopropyl-1-thio- $\beta$ -D-galactopyranoside (IPTG) for 3 h (Figures 2A and 3A). Of note, the fusion proteins accounted for an estimated 25% of total bacterial protein. By contrast, expression of the ProIAPP- and mutProIAPP-alone constructs did not result in detectable target protein (data not shown). Thus, this approach was not pursued further. Both fusion proteins partitioned with the insoluble lysate fraction and formed inclusion bodies. Inclusion bodies were solubilized in 6 M urea (Figures 2A,B and 3A,B) and fusion proteins were then purified by ion metal affinity chromatography (IMAC) under denaturing, i.e. urea-containing, conditions (Figure 2A). IMAC eluates from both fusion proteins were approximately 80% pure (Figure 2A) and were further purified to homogeneity by reverse phase

(RP)-HPLC on a C<sub>18</sub>-column. After this step, the Trx fusion proteins which eluted within sharp peaks at about 24 min were judged as highly homogeneous on the basis of their sodium dodecyl sulfate–polyacrylamide gel electrophoresis (SDS–PAGE) (Figure 2F) and HPLC profiles (Figures 2C and 3C). HPLC-purified fusion proteins were further characterized by matrix-assisted laser desorption ionization–time-of-flight–mass spectroscopy (MALDI-TOF-MS) which confirmed their identity and high grade of purity. The MS data suggested that the applied expression system produced the fusion proteins both in an unprocessed form and with the N-terminal Met-residue cleaved. Cleavage of the N-terminal Met was mainly dependent on the induction conditions, i.e. length of bacterial growth and IPTG concentration. For fusion proteins without Met, the following masses were determined: Trx-ProIAPP, 24 456  $\pm$  24 Da (M+H<sup>+</sup>) compared to an expected mass (M+H<sup>+</sup>) of 24 430 Da; Trx-mutProIAPP, 24 125  $\pm$  24 Da (M+H<sup>+</sup>) compared to a theoretical mass (M+H<sup>+</sup>) of 24 145 Da. For protein species with the Met residue included, representative masses for several preparations were: Trx-ProIAPP, 24 601  $\pm$  25 Da (M+H<sup>+</sup>) and Trx-mutProIAPP, 24 238  $\pm$  48 Da (M+H<sup>+</sup>) compared to the expected values of 24 561 Da (M+H<sup>+</sup>) and 24 276 Da (M+H<sup>+</sup>), respectively.

Ek cleavage of Trx-ProIAPP resulted in an SDS–PAGE electropherogram with a total of six detectable bands, likely representing residual uncleaved fusion protein, the cleaved Trx-Tag, monomeric ProIAPP, and also dimeric, trimeric and multimeric ProIAPP self-assemblies (Figure 2A). This notion was confirmed by HPLC and mass spectroscopy (MS) analysis of the Ek digests (Figure 2D). Although unexpected at first sight, stable non-covalent oligomer formation even under SDS-based denaturing conditions has often been observed for amyloid polypeptides [12,28]. Consistent with the notion that stable oligomerization of ProIAPP had occurred, was the finding that the cleaved Trx-Tag band (identity confirmed by MS at a mass of 17 069  $\pm$  17 Da (M+H<sup>+</sup>); expected: (M+H<sup>+</sup>) of 17 045 Da) was much stronger than any single ProIAPP band, in particular the presumed monomer band. Together, these observations already argued that ProIAPP had a strong tendency to self-assemble into oligomers.

Digests were then subjected to C<sub>18</sub>-HPLC purification (Figure 2D). Cleaved ProIAPP was well separated from both the remaining uncleaved fusion protein and the Trx-Tag and was isolated and lyophilized (Figure 2D). SDS–PAGE and MS analysis of the HPLC fractions (Figure 2F and data not shown, respectively) confirmed their correct assignment. The high purity grade of HPLC-purified ProIAPP was further confirmed by HPLC and MS (found (M+H<sup>+</sup>): 7549  $\pm$  8 Da; calculated: (M+H<sup>+</sup>) 7517 Da). Of note, we were unable to detect monomeric ProIAPP by SDS–PAGE when eluates of the HPLC puri-

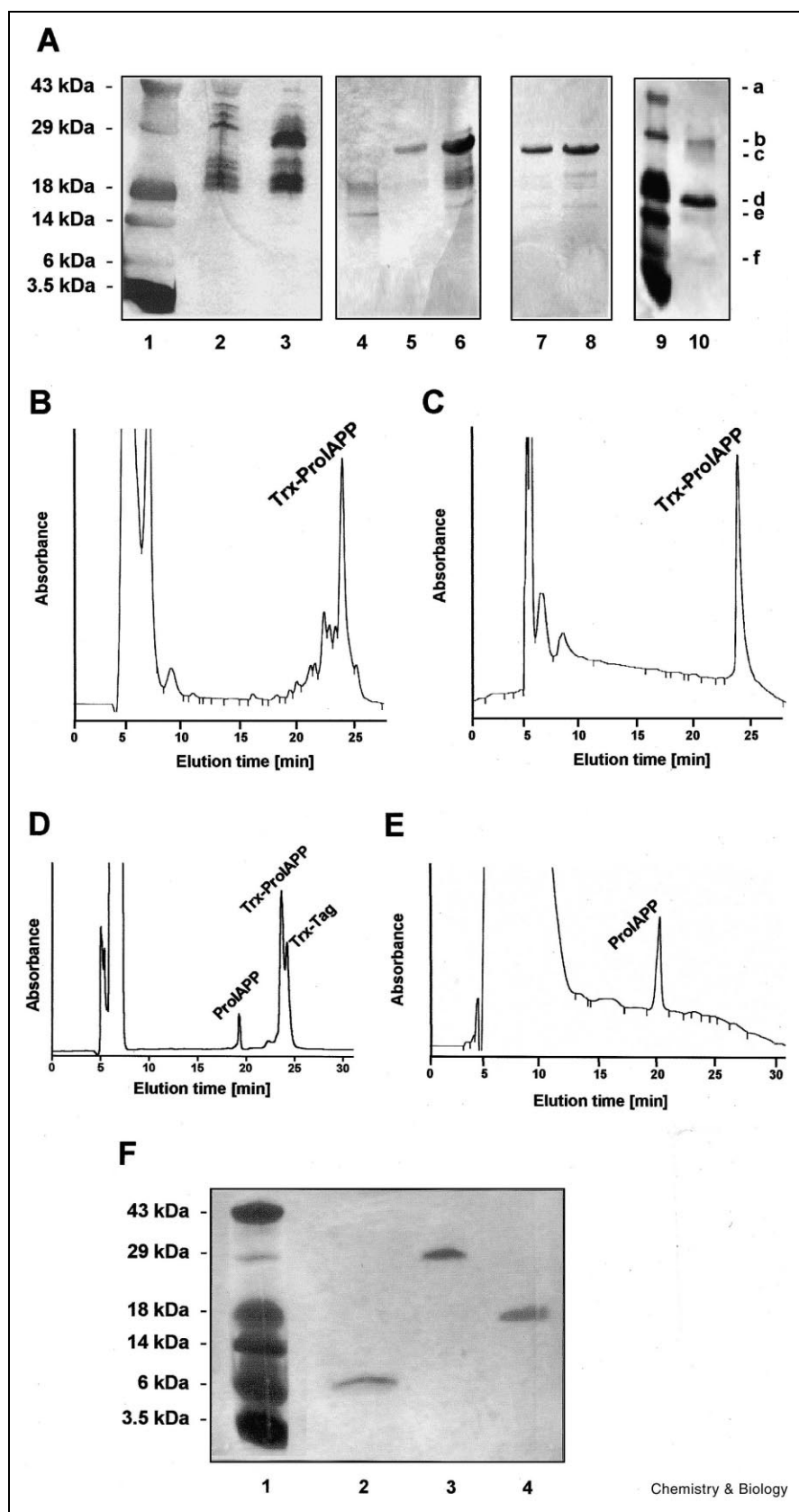


**Figure 2.** Expression and purification of ProlAPP. **(A)** SDS-PAGE of the expression, His-Tag-based purification and Ek cleavage of the Trx-ProlAPP fusion protein. The fusion protein was expressed by bacterial overexpression and crude lysates and processed preparations electrophoresed in a 20% homogeneous gel. Comparable protein quantities were applied in each lane. A molecular weight marker of the indicated size range was co-analyzed (lanes 1 and 9). Lane 2: uninduced control; lane 3: crude extract from IPTG-induced culture; lane 4: soluble fraction of the lysate; lanes 5 and 6: urea-solubilized inclusion body fraction at a protein quantity as in 4 and at a five-fold higher amount; lanes 7 and 8: first and second eluate fractions of His-Tag chromatographic step; lane 10: Ek-digested His-Tag column eluate; letters a-f indicate the putative ProlAPP species identified and correspond to a ProlAPP oligomer, the uncleaved fusion protein, a ProlAPP trimer, the Trx-tag, a ProlAPP dimer, and the ProlAPP monomer, respectively. **(B)** RP-HPLC chromatogram of a urea-solubilized inclusion body fraction of Trx-ProlAPP (for HPLC conditions, also for (C)-(E), see Materials and Methods). The peak at 5-10 min is due to urea. **(C)** RP-HPLC chromatogram of HPLC-purified Trx-ProlAPP dissolved in 10% HAc. The peak at 5-10 min is due to HAc. **(D)** RP-HPLC chromatogram of an Ek-digested preparation of HPLC-purified Trx-ProlAPP. The identified polypeptide species are indicated. **(E)** RP-HPLC chromatogram of HPLC-purified ProlAPP dissolved in 10% HAc. The peak at 5-10 min is due to HAc. **(F)** SDS-PAGE of the HPLC-purified and lyophilized fractions as recovered from (D). The marker (lane 1) was as in (A). Lanes 2-4 represent the ProlAPP, fusion protein and tag peaks, respectively.

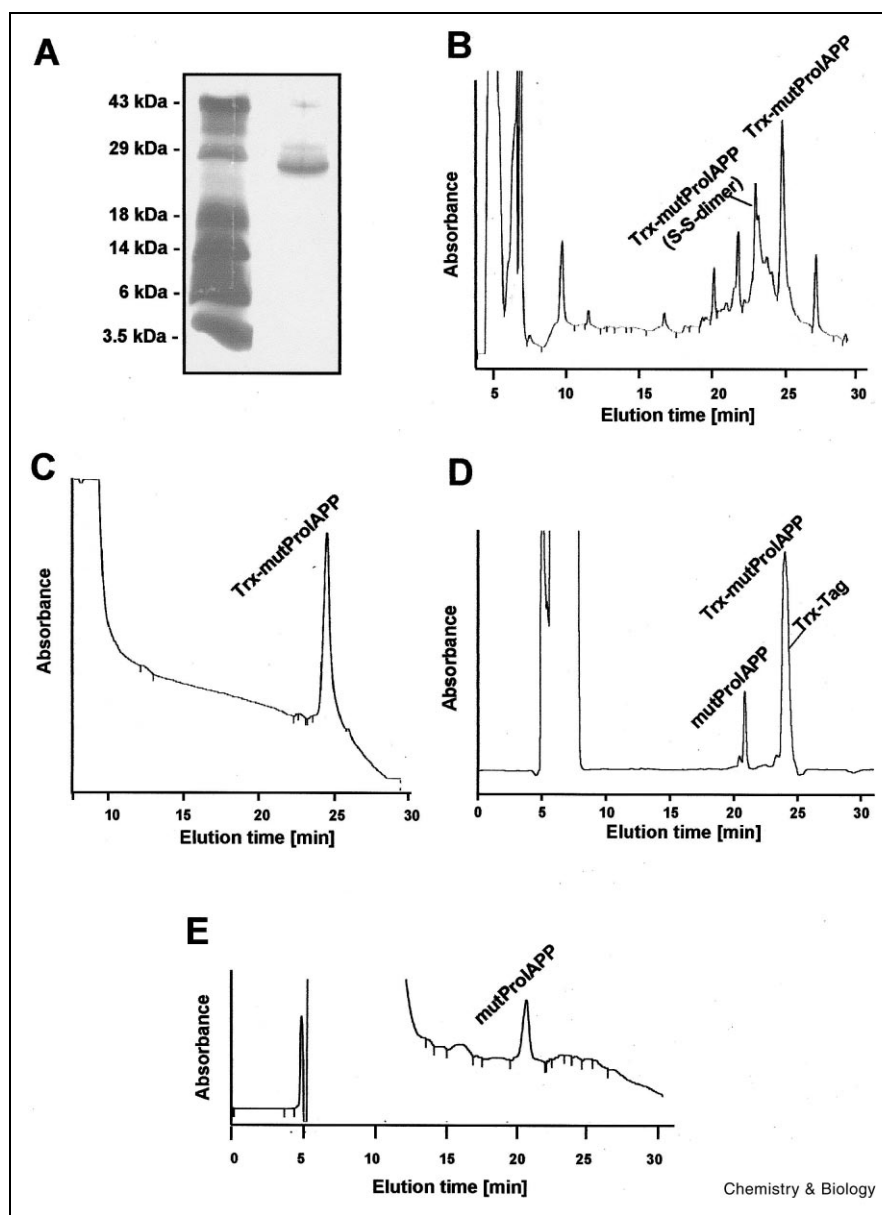
fications were directly subjected to SDS-PAGE analysis. Instead, only bands likely corresponding to higher molecular weight ProIAPP aggregates were obtained under these conditions. However, ProIAPP in its monomeric form (see Figure 2F), was always detected when the collected HPLC fractions were immediately frozen and lyophilized and then directly dissolved in the SDS sample buffer, boiled and electrophoresed immediately. Similar observations were made during attempts to recover ProIAPP by C<sub>18</sub>-HPLC, indicating a strong and time-dependent aggregational potential for monomeric ProIAPP.

In summary, from 200 ml bacterial culture, 42 mg of total bacterial lysate protein and 5 mg of pure Trx-ProIAPP

fusion protein were recovered, corresponding to an overall yield of 12.5%. Following Ek cleavage, HPLC purification yielded 0.9 mg of pure ProIAPP, which corresponded to a Trx-ProIAPP cleavage and purification yield of 60%. It is of note that the established recombinant procedure enables the purification of several milligrams of pure Trx-ProIAPP fusion protein and pure ProIAPP from a few liters of culture within 1 week.

Ek cleavage of HPLC-purified Trx-mutProIAPP (Figure 3C) proceeded essentially as described for the wt fusion protein according to SDS-PAGE (data not shown), HPLC (Figure 3D) and MS analyses of the digests. Following HPLC purification of the digests, mutProIAPP of high

**Figure 3.** Expression and purification of mutProIAPP (for conditions see Figure 2). **(A)** SDS-PAGE (20% homogeneous gel) of a Trx-mutProIAPP-containing inclusion body fraction. Trx-mutProIAPP was expressed and processed as for Trx-ProIAPP (see legend of Figure 2A). Left lane: A molecular weight marker of the indicated size range was co-analyzed; right lane: urea-solubilized inclusion body fraction. **(B)** RP-HPLC chromatogram of urea-solubilized inclusion bodies of Trx-mutProIAPP. The S-S-dimeric Trx-mutProIAPP adduct was identified by MS (see Results). The peak between 5–10 min is due to urea. **(C)** RP-HPLC chromatogram of HPLC-purified Trx-mutProIAPP dissolved in 10% HAC. The peak between 5–10 min is due to HAC. **(D)** RP-HPLC chromatogram of an Ek-digested preparation of HPLC-purified Trx-mutProIAPP. The peak between 5–10 min is due to HAC. The identified proteins as confirmed by MS are indicated. The Trx-Tag has a nearly identical retention time to Trx-mutProIAPP under the applied HPLC conditions. **(E)** RP-HPLC chromatogram of HPLC-purified mutProIAPP dissolved in 10% HAC. The peak between 5–12 min is due to HAC.



purity was obtained as confirmed by HPLC (Figure 3E) and MS analysis of the HPLC-collected mutProIAPP peak (found  $(M+H^+)$  mass:  $7238 \pm 7$  Da; calculated  $(M+H^+)$  mass: 7233 Da). All chromatographic purifications of mutProIAPP and its fusion protein led to reduced recovery yields compared to the corresponding wt species. One reason for this finding appears to be the observed propensity of Trx-mutProIAPP, solubilized from inclusion bodies by aqueous 6 M urea, to oxidize into disulfide-linked di- and oligomers, even during storage at  $-20^\circ\text{C}$  in buffer containing 6 M urea (Figure 3B). The formation of such species was derived from MS analyses of the corresponding HPLC fractions (Figure 3B). Of note, formation of the disulfide species was reversible by treatment with dithiothreitol. Trx-ProIAPP was also found to be prone to oxidation under the above conditions, but to a lesser degree than the mutant protein. In addition, increased adherence of mutProIAPP-related proteins as compared to the ProIAPP-derived species on the chromatographic support was noted. This behavior could be due to the predicted higher hydrophobicity of mutProIAPP (see above). Overall and likely owing to the discussed effects, mutProIAPP recovery from the last purification step was about 25% of that obtained for ProIAPP.

#### Amyloidogenicity of ProIAPP, mutProIAPP and the fusion proteins

We aged ProIAPP, mutProIAPP and the fusion proteins for four days under the fibrillogenic conditions previously established for native-like amyloid formation by IAPP [12,13,29]. The resulting solutions were then tested for amyloidogenic properties.

Both Trx-ProIAPP and ProIAPP bound CR [30]. However, only ProIAPP exhibited the green-yellow birefringence (Figure 4A) that CR-treated amyloid structures, including IAPP fibrils [13], usually exhibit under polarized light [30]. MutProIAPP and Trx-mutProIAPP bound CR, but did not show birefringence under polarized light (data not shown).

EM analysis revealed that aged ProIAPP solutions consisted of fibrils and fibril bundles with the typical morphology of amyloid (Figure 4B). ProIAPP fibrils had diameters between 10 and 20 nm and consisted of at least two filaments that coiled around each other, yielding fibrils that showed an axial helical periodicity [10,31,32]. Mutated ProIAPP also formed fibrils (Figure 4C). Compared to ProIAPP, the fibrils of the mutant protein formed a web-like structure that was denser than that of ProIAPP, while

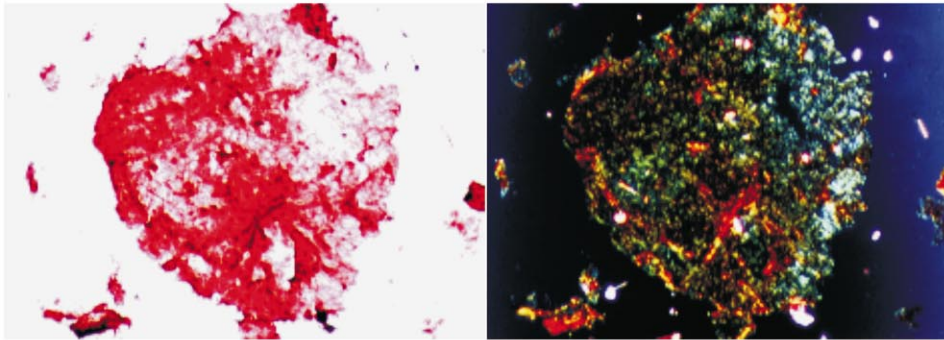
single fibrils appeared to have diameters of the same order as those of ProIAPP. Of importance, our findings indicated that there are no marked differences between the morphological features of ProIAPP and IAPP fibrils when prepared under the same fibril-promoting conditions (Figure 4B,D). However, IAPP fibrils are usually visibly insoluble while ProIAPP fibrils were not visible to the eye, indicating that higher-order fibrillar aggregates form in the IAPP solution. In addition, a number of the observed ProIAPP fibrils were shorter (average length of less than 700 nm) than usually found IAPP fibrils. Contrary to ProIAPP and mutProIAPP, the Trx fusion proteins did not form fibrils (Figure 4E).

#### Solution conformation of ProIAPP, mutProIAPP and the fusion proteins as determined by CD spectroscopy

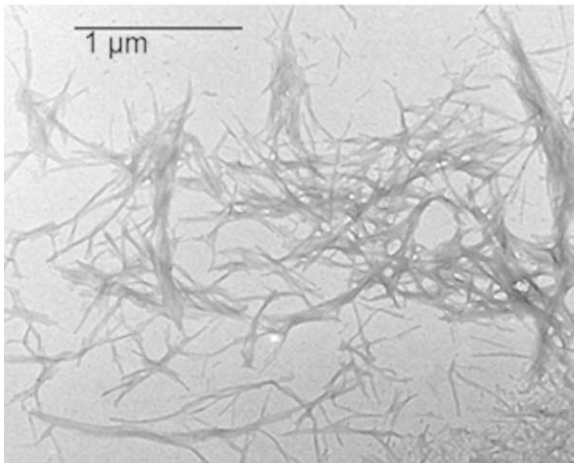
We next studied the conformation of the investigated proteins in solution by far-UV CD spectropolarimetry. To be able to study the solution conformation of a protein with amyloidogenic potential, appropriate stock solutions that keep the protein in a non-aggregated and denaturated state are required [13,22,33,34]. 1,1,1,3,3,3-Hexafluoro-2-propanol (HFIP) is a commonly used solvent that keeps amyloidogenic polypeptides in a disaggregated and denaturated state [13,33] and has been used previously by us to prepare IAPP stocks [12,13]. Unfortunately, ProIAPP was completely insoluble in HFIP. We thus applied 8 M urea to prepare stocks of ProIAPP, mutProIAPP, and the fusion proteins and found that these conditions kept the proteins in a soluble and non-aggregated state (at 500  $\mu\text{M}$  and  $-20^\circ\text{C}$  for several months). To compare the results of these studies with the results of our previous studies on IAPP [13] stocks of IAPP in 8 M urea were also prepared and comparative CD experiments performed with IAPP under the same buffer conditions as for the pro-proteins. The need to use urea stocks for IAPP was accompanied by several experimental difficulties. For example, like the previously investigated denaturant guanidine hydrochloride (GdnHCl) [13], urea proved not to be an ideal denaturant for IAPP. Variable lag times were obtained when IAPP stocks in 8 M urea were used to prepare the CD solutions which was in contrast to the recently reported measurements using HFIP stocks [13]. Aggregational lag times were found to depend on several factors, including the 'age' of the stock solution. This observation may be related to the degree of unfolding caused by urea and a possible stabilization of partially unfolded amyloidogenic populations as previously found to occur in GdnHCl solutions [13]. This suggestion would be consistent with the observed increased  $\beta$ -sheet contents of IAPP in the urea-con-

**Figure 4.** ProIAPP and mutProIAPP but not the corresponding fusion proteins are amyloidogenic. In (A) CR staining of aged ProIAPP is shown: on the left, bright field microscopic examination; on the right microscopic examination under polarized light are shown. EM analysis of negatively stained, aged solutions of ProIAPP (B), mutProIAPP (C), IAPP (D) and the Trx-ProIAPP fusion protein (E) are shown. EM pictures of Trx-mutProIAPP preparations were identical to that shown in (E). All proteins were aged in 10% HAc as described in Materials and Methods and analyses were performed with a protein working concentration of 1 mM. Size bars for the EM pictures are indicated.

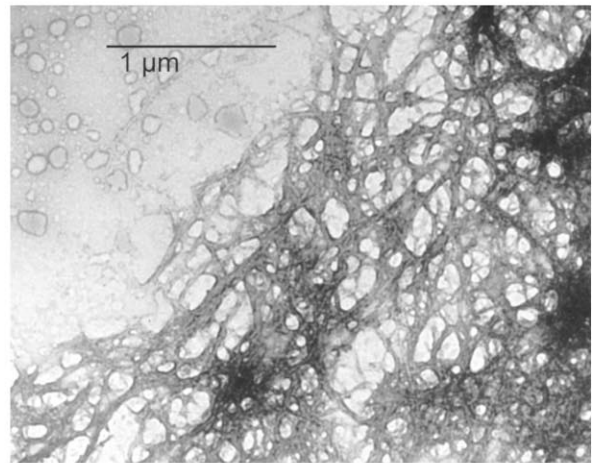
**A**



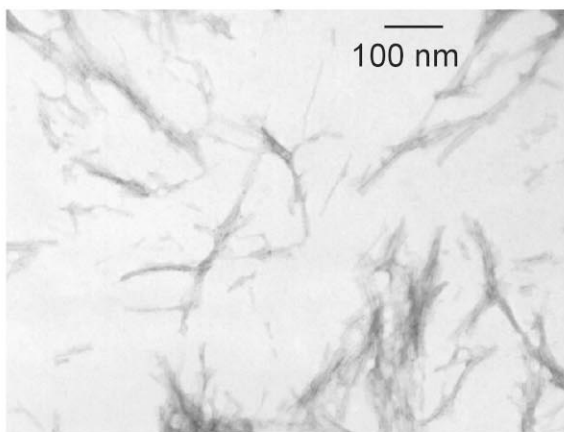
**B**



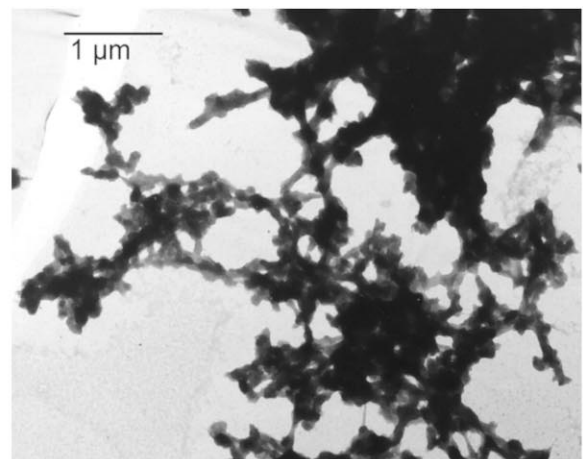
**C**



**D**



**E**



taining buffer as compared to HFIP conditions (see below). More detailed investigations on the effect of urea on IAPP unfolding and amyloidogenicity are needed but are not the focus of this study.

We first confirmed that the denatured proteins immediately refolded upon 100-fold dilution of the denaturant into the CD buffer [35]. Protein refolding was evident from the lack of time-dependent changes in the CD spectra for up to 5 h and was in agreement with the often described rapid folding of polypeptides. We found no concentration dependence in the spectra of ProIAPP between 0.5 and 5  $\mu\text{M}$ . This indicated that ProIAPP was predominantly monomeric over this concentration range, at least immediately following preparation of the solution. Self-assembly was observed to occur only hours later (see below).

Spectra of ProIAPP and mutProIAPP were then recorded at protein concentrations of 5  $\mu\text{M}$  in 10 mM phosphate buffer containing 0.08 M urea. Such a urea concentration was unlikely to have an effect on protein conformation, as no changes in the CD spectra were observed upon a 1/10 dilution of these solutions into phosphate buffer (resulting urea concentration of 0.008 M). CD spectra of the fusion proteins were measured at a protein concentration of 1  $\mu\text{M}$  and in the same buffer as above.

The CD spectrum of freshly reconstituted ProIAPP showed a strong minimum at about 208 nm (Figure 5A), indicating that the protein contained considerable portions of both ordered and random coil structure. This result was confirmed by multilinear regression analysis of the spectra by using the Lincomb program [36] and the reference

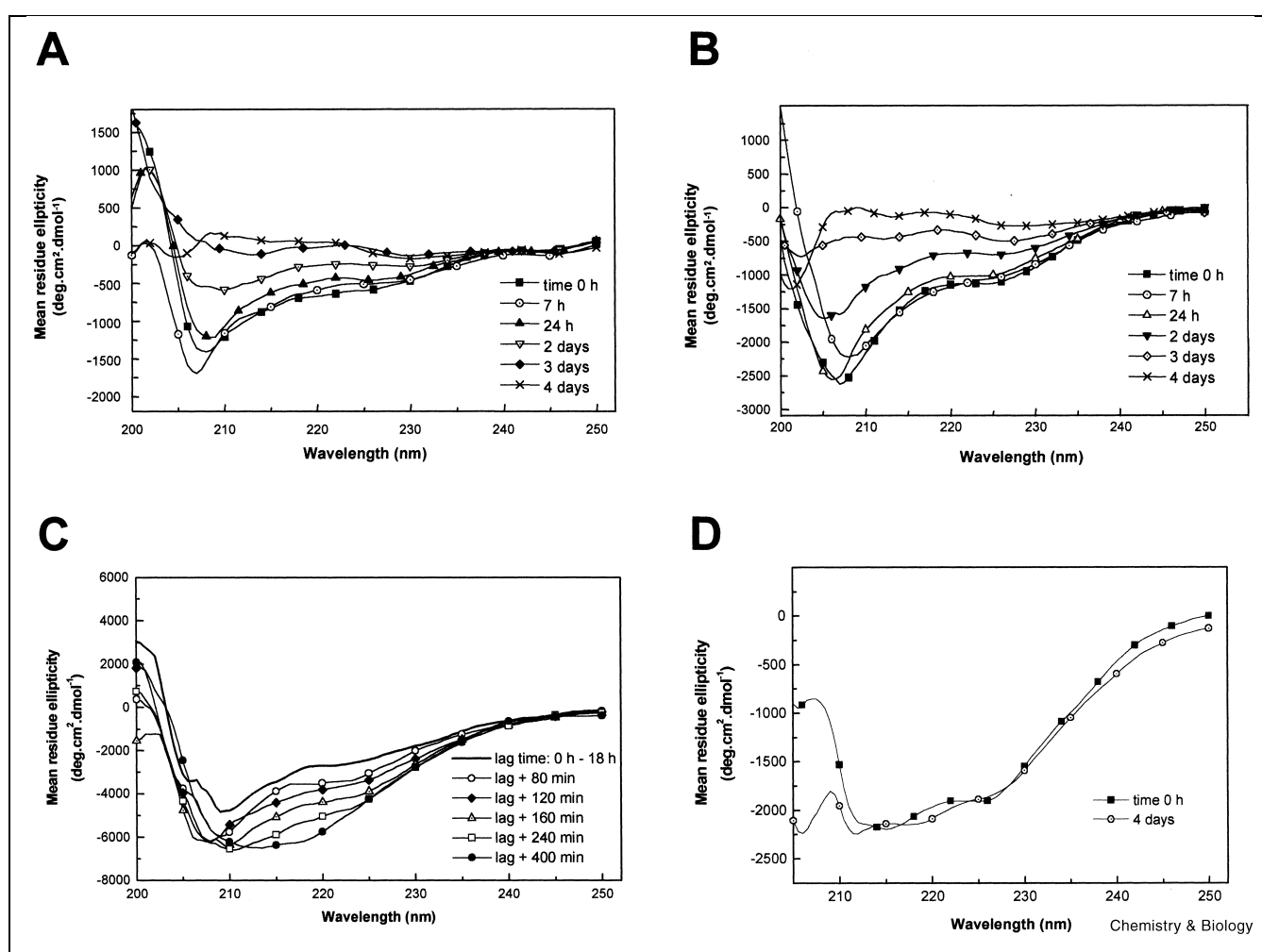


**Figure 5.** Aging of the proteins as followed by CD spectroscopy. Far-UV CD spectra of freshly dissolved and aged ProIAPP (A), mutProIAPP (B), IAPP (C), and the Trx-ProIAPP fusion protein (D). CD spectra were obtained at the indicated time points in protein solutions containing 5  $\mu\text{M}$  protein (1  $\mu\text{M}$  in D) in 10 mM sodium phosphate buffer and 0.08 M urea, pH 7.4, as described in Materials and Methods.

spectra sets of Perczel et al. [36] and Brahms and Brahms [37]. According to these analyses, folded ProIAPP contained approximately 50% structured elements that consisted of  $\beta$ -sheets and  $\beta$ -turns. Antiparallel  $\beta$ -sheet structure was the dominant (50%) structured element according to the reference set of Perczel et al., while analysis by Brahms and Brahms suggested the presence of both  $\beta$ -sheets (30%) and  $\beta$ -turns (20%). Refolded mutProIAPP had a very similar spectrum (Figure 5B) to that of ProIAPP, indicating that the introduced mutations did not significantly affect the overall conformation of ProIAPP. It should be noted that the set of Perczel et al. encompasses reference spectra for parallel  $\beta$ -sheets and also reference spectra for antiparallel  $\beta$ -sheet structure [36,38]. By contrast, the set of Brahms and Brahms cannot differentiate between these two structures [37]. However, since the CD of  $\beta$ -sheets may strongly vary depending on the various features of the sheets [39], a distinction between the two types of  $\beta$ -sheet structure should be interpreted with caution. The spectrum of Trx-ProIAPP was similar to that of ProIAPP (Figure 5D). Deconvolutions indicated that  $\beta$ -sheets and  $\beta$ -turns were the predominant ordered elements in Trx-ProIAPP (40–55%). The shape of the CD spectrum of IAPP in the 0.08 M urea-containing buffer indicated the presence of significant amounts of structured elements in addition to the random coil component (Figure 5C). This notion was confirmed by deconvolutions, which suggested that the ensemble of conformations of IAPP consisted predominantly of  $\beta$ -sheets (40–50%), with about 50% of un-ordered elements present.

We have recently reported that, at 45°C, IAPP populates a conformeric state that is able to immediately self-assemble into  $\beta$ -sheets and insoluble amyloid [13]. Temperature-induced denaturation of ProIAPP and mutProIAPP was thus studied next. Interestingly, the overall conformations of both ProIAPP and mutProIAPP were found to be essentially independent of temperature (up to 95°C). No evidence was obtained that a specific ProIAPP conformeric state was populated in the temperature denaturation pathway (data not shown) and no amyloid formation was observed during denaturation of ProIAPP and mutProIAPP.

#### **Aging of ProIAPP, mutProIAPP, and the fusion proteins as followed by CD and EM**

We applied far-UV CD in combination with EM and followed the effect of ‘aging’ on ProIAPP, mutProIAPP and fusion protein conformation and amyloidogenicity. For comparison, ‘aging’ studies under the same conditions were also performed for IAPP.

Freshly refolded aqueous protein solutions at 5  $\mu$ M were allowed to stand in the CD cell for several days at room temperature (RT) and spectra were measured at various time points [13] (Figure 5). The spectrum of ProIAPP (Figure 5A) started to change 7 h following refolding.

This change was characterized by a red shift of the minimum at 207 nm that reached 212 nm 3 days later and by a dramatic (absolute) decrease of the magnitude of the overall CD signal. After four days, nearly no CD signal was present in the aged ProIAPP solution. A nearly identical conformational transition was seen during the aging process of mutProIAPP (Figure 5B). The dramatic reduction in the CD signal may have been due to protein precipitation or adsorption by the glass surface of the quartz cell [12,40]. It appears, however, that neither of these effects had accounted for the observed changes. First, the absorbance of the protein solution in the UV region (200–250 nm) did not change during the time scale of the experiment. Secondly, no turbidity, protein insolubilization, or precipitation was noted during the experiments. Thirdly, no concentration effect was observed when ProIAPP was measured at a 10-fold lower concentration (0.5  $\mu$ M), which usually would be a characteristic feature of loss of CD signal due to adsorption to the glass surface [40]. These results suggested that the time-dependent changes in the CD spectra of ProIAPP and mutProIAPP were due to real aging-related conformational transitions. Such changes may occur during ProIAPP or mutProIAPP oligo- and multimerization. This notion would be consistent with the observation that we were unable to detect reasonable amounts of monomers of ProIAPP or mutProIAPP when the CD solutions were subjected to SDS-PAGE (not shown).

CD time-dependence studies of IAPP were then performed (Figure 5C). These data confirmed that also under these conditions, IAPP aggregation into amyloid proceeded via the recently described conformational transition into  $\beta$ -sheets [13]. The transition started following a lag time that varied from 0 to 18 h.

The spectra of the fusion proteins did not change over time (Figure 5D) and monomers of these species were readily detectable by SDS-PAGE, confirming that these proteins had a strongly diminished self-association potential compared to ProIAPP or mutProIAPP.

The aged CD solutions were centrifuged and pellets examined by EM. ProIAPP pellets (after 5–6 days of aging) were found to contain areas that consisted of either non-fibrillar yet ordered self-assembled species (Figure 6A) or of fibrillar assemblies (Figure 6B). The non-fibrillar species (Figure 6A) seemed to consist of at least all three prefibrillar oligo- and multimeric species that have recently been described to appear early in the amyloidogenesis process of  $\alpha$ -synuclein and  $\beta$ -amyloid peptide (A $\beta$ ) [41–43]. The species included: (a) spherical species, that have previously been named ‘spheres’ (estimated diameters between 10 and 20 nm) and which seemed to be the basic units of the observed ordered, non-fibrillar assemblies; (b) linear assemblies that appeared to consist of a linear association of ‘spheres’ and that could be identical to the so-called

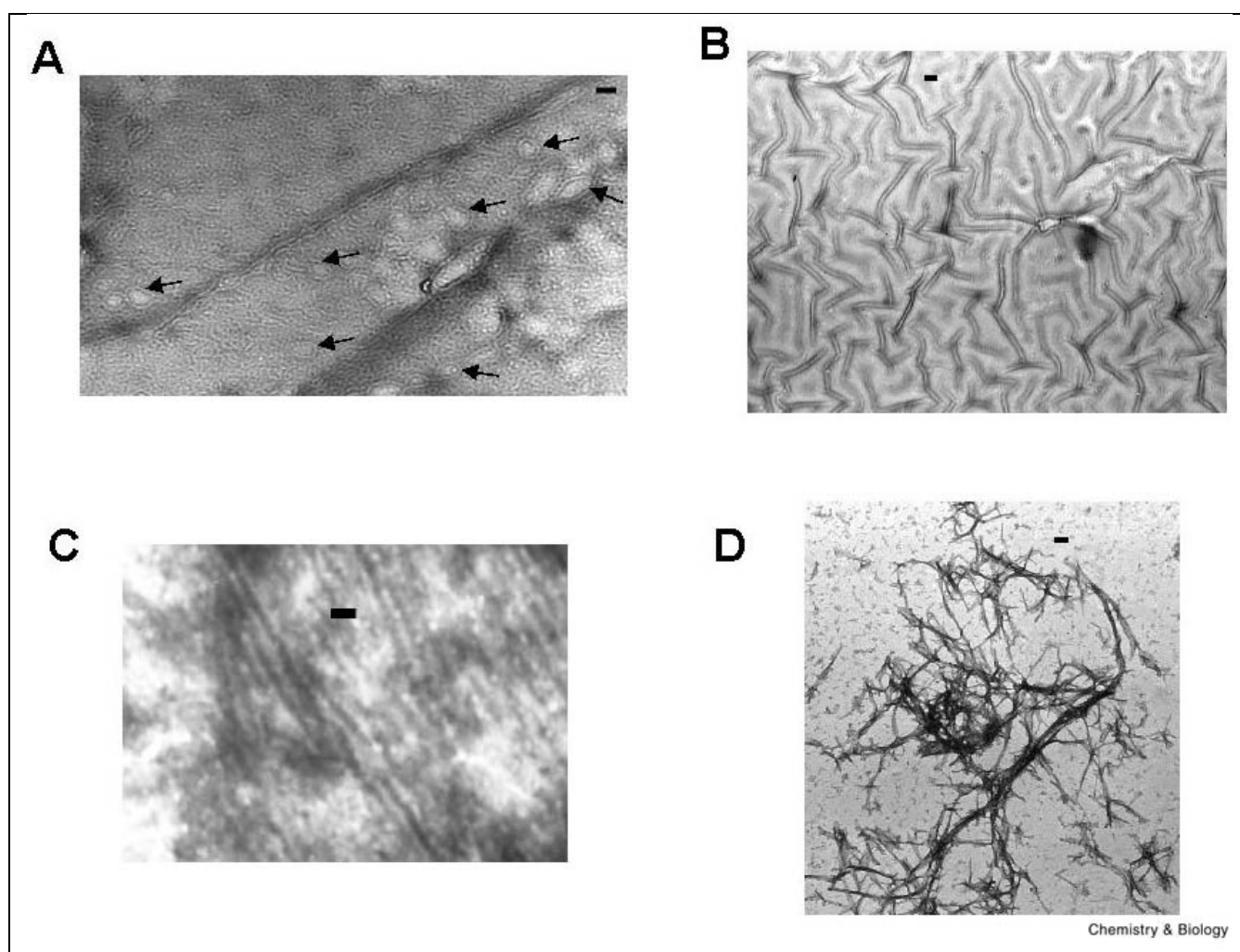


**Figure 6.** Electron microscopic examination of the aggregates formed following aging of CD solutions of ProIAPP (**A**, **B**), mutProIAPP (**C**) and IAPP (**D**). Protein concentrations were 5  $\mu$ M in 10 mM phosphate buffer containing 0.08 M urea, pH 7.4. In (**A**), the ordered but non-fibrillar ProIAPP aggregates are shown (arrows indicate 'ring'-like structures) and in (**B**), fibrillar ProIAPP aggregates are shown. The above assemblies represent the main species present 5–6 days after the start of the incubation. In (**C**), fibrillar mutProIAPP aggregates are shown that represent the fibrillar species that were present 5–6 days after the start of the incubation. Major parts of the grid were covered by amorphous aggregates which are not shown. In (**D**), IAPP fibrils that were representative of the fibrillar species obtained 48 h following the start of the incubation are shown. Note that aging of the protein preparations used, was followed up by CD prior to the EM analysis

'chains' or 'protofibrils' [41–43] and (c) 'chains', that appeared circularized into the recently identified 'rings' [41] and which were either elliptical or circular. Of note, assemblies of two-, four-, and six-'ring' structures that appeared to be similar to the 'loops' recently reported to be present in apolipoprotein C-II amyloid aggregates were also observed [44]. The diameters of the circular assemblies were estimated to be between 30 and 60 nm, while for the elliptical structures, axes of about 40–60 nm by 70–150 nm were estimated.

The fibrillar assemblies found were not visible to the eye and had similar diameters to ProIAPP fibrils that were observed when fibrillogenic, high-concentration incubation

conditions were applied (Figure 4B). Fibrils were of various lengths and partly assembled laterally into broad, sheet-like arrays (Figure 6B). Several of the fibrils intertwined at several cross-sections with others leading to an extension of the fibrillar array over several square micrometers (Figure 6B). These fibrillar assemblies were different from the typical fibrillar bundles seen under 'fibrillogenic' conditions (Figures 4B and 6B).

Pellets of the CD incubations of mutProIAPP (incubated for 5–6 days) also contained some transparent, sheet-like fibrillar arrays which mainly consisted of laterally associated fibrils (Figure 6C). Unlike for ProIAPP, major parts of the grid were covered by amorphous aggregates.

IAPP pellets obtained from the CD experiments following the transition into  $\beta$ -sheets (Figure 5C) were also examined. These preparations mainly contained insoluble amyloid fibrils and fibrillar bundles of typical amyloid appearance (Figure 6D) while protofibrils [11,42] and ordered oligomers were also present (Figure 6D).

### Cytotoxicity of ProIAPP, mutProIAPP and the fusion proteins on a pancreatic cell line

IAPP-derived amyloid is strongly cytotoxic to a variety of cells, including pancreatic  $\beta$ -cells [6,22]. We compared the potential cytotoxicity of aged ProIAPP and mutProIAPP solutions with the cytotoxicity of IAPP on the pancreatic cell line RIN5fm [6,21–23].

The aged stock solutions applied (2 mM protein in 10% HAC, 4 days incubation followed by neutralization with 10%  $\text{NH}_4\text{OH}$ ) were analyzed by EM prior to the cellular assay and were found to predominantly contain amyloid fibrils (Figure 4B–D). Serial dilutions of these stocks with cell medium were then made to obtain apparent protein concentrations from 1  $\mu\text{M}$  to 10 nM. The term ‘apparent concentration’ is an approximation and relates to the molar concentrations of these proteins in a non-associated state [22]. IAPP was cytotoxic with an obtained  $\text{EC}_{50}$  of about 100 nM, while aged ProIAPP was also found to be cytotoxic, but was about three-fold less toxic than IAPP ( $\text{EC}_{50}$  of  $\sim 300$  nM) (Figure 7). Interestingly, aged mutProIAPP solutions showed essentially no cytotoxic properties (Figure 7). The non-amyloidogenic fusion proteins

fully lacked cytotoxicity (data not shown).

Although the fibrillar state of ProIAPP and mutProIAPP in the stock solutions used to prepare the diluted samples was demonstrated by EM (see Figure 4B,C), the compositions of their assembly states at the lower concentrations as applied onto the cells were not known. Consistent with previous findings [13], significant amounts of fibrillar aggregates were found in diluted IAPP solutions including the 1  $\mu\text{M}$  solution (not shown). However, EM examination after 1 day of incubation of a 10  $\mu\text{M}$  ProIAPP solution (made by dilution into 10 mM phosphate buffer, pH 7.4, of the fibrils of the 2 mM ProIAPP incubation (see above)) failed to detect fibrillar species while ordered, oligomeric assemblies and amorphous aggregates were present. By contrast, at 100  $\mu\text{M}$  ProIAPP, sheet-like fibrillar assemblies (Figure 6B) were seen. In the case of diluted mutProIAPP fibrils, mainly amorphous aggregates and some non-fibrillar, ordered oligomers were detected at protein concentrations equal to or less than 100  $\mu\text{M}$ .

### Discussion

We elected to generate human ProIAPP and mutProIAPP by recombinant methods rather than chemical synthesis. As the IAPP molecule is among the most amyloidogenic peptides known, the chemical synthesis of ProIAPP by methods of solid phase peptide synthesis (SPPS) was predicted to be difficult [10,13,18,19,28]. Recombinant expression of polypeptides that, by length, are still within the reach of SPPS methods have recently been applied more widely, because efficient recombinant expression systems have become available [18,27,45]. Another reason for the recombinant strategy chosen for this study was that we wished to generate fusion proteins with the ProIAPP moiety linked to a soluble protein tag that could serve to enhance solubility [27,46].

The Trx-tagged fusion proteins were expressed successfully at good rates. Trx-based gene fusion expression systems have proven useful for the convenient expression and purification of weakly soluble proteins [27,47]. There are some examples of successful recombinant expression of an amyloid polypeptide as fusion construct with a soluble protein moiety. These include the expression of the  $\text{A}\beta$  peptide as Trx–His-tagged fusion construct [18], the expression of the Ure2 prion domain (UPD) as glutathione-*S*-transferase (GST)–UPD fusion protein [48], or the expression of the Huntington’s disease (HD) protein as GST–HD exon 1 fusion protein [49,50]. Our study is the first example of recombinant expression of an IAPP-related protein. As for the other reported examples, expression of ProIAPP as a fusion construct together with a soluble moiety offered several advantages. We obtained good expression rates (approximately 25%); the fusion protein partitioned with the inclusion body fraction, but could be solubilized and handled thereafter; and following cleavage,

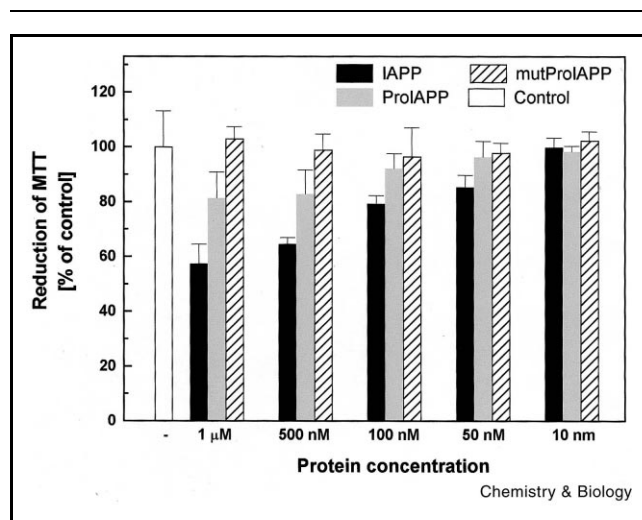


**Figure 7.** Cytotoxicity potentials of ProIAPP and mutProIAPP in comparison to IAPP. Aged protein solutions were added to RIN5fm pancreatic islet cells at the indicated concentrations and cell viability assessed by MTT reduction assay after a 20 h incubation. Data are percentage values of control (vehicle alone; 100% viability) and represent the mean  $\pm$  S.D. from 6–18 determinations.

we obtained ProIAPP in reasonable amounts and good purity. Most importantly, isolated ProIAPP exhibited properties that were, although distinct from IAPP, that of an amyloidogenic polypeptide, demonstrating that the recombinant expression and reconstitution procedure allowed for the properties of ProIAPP to be retained.

The Ek cleavage designed to proceed C-terminally of the recognition sequence (Asp)<sub>4</sub>-Lys in Trx-ProIAPP and Trx-mutProIAPP was generally found to be specific. However, we occasionally observed formation of a non-specific cleavage product. According to MS analysis, this by-product (amounting to 0–30% of ProIAPP or mutProIAPP yield) corresponded to the sequence stretch [23–67], thus likely having resulted from Ek cleavage at the Arg<sup>22</sup>-Leu<sup>23</sup> amide bond of either protein. For the non-specific cleavage product of ProIAPP a (M+H<sup>+</sup>) mass of 4914 ± 5 Da was found (calculated (M+H<sup>+</sup>) mass: 4921 Da) and for the side-product of mutProIAPP a (M+H<sup>+</sup>) mass of 4778 ± 5 Da was measured (calculated (M+H<sup>+</sup>) mass: 4778 Da). The similarity of sequence Asn<sup>21</sup>-Arg<sup>22</sup>-Leu<sup>23</sup> to the Ek cleavage recognition site (Asp)<sub>4</sub>-Lys-Ile might thus have accounted for the observed non-specific cleavage. Our current data indicate that the non-specific cleavage may have been due to the use of an excess of Ek and prolonged cleavage times that were occasionally applied to increase the yields of ProIAPP or mutProIAPP.

Removal of the fusion protein moieties led to a dramatic change in protein solubility as well as aggregational and amyloidogenic potential (see below). ProIAPP and mutProIAPP were found to aggregate into fibrils of typical amyloid morphology, when the amyloid-promoting conditions were applied that have previously been used to generate native-like IAPP fibrils [13,29]. Similar to IAPP fibrils, ProIAPP fibrils exhibited birefringence under polarized light following staining with CR. By contrast, mutProIAPP fibrils did not show birefringence. The exact mechanism of CR binding and birefringence of amyloidogenic polypeptides is still unknown [34]. In addition, there have been several reports about fibrils of various proteins that lack birefringence upon CR staining [51–53]. One reason for the observed different CR behavior of ProIAPP and mutProIAPP could lie within different ratios of fibrillar (which most probably are the birefringent species) to non-fibrillar aggregates (which are usually not birefringent [54]) present in the CR incubations which may be caused by differences in fibrillar stability and fibril dissociation rates into aggregates. This has been recently suggested to account for the reduced CR binding of Aβ protofibrillar species as compared to the corresponding fibrils [54]. Here, such a notion would be consistent with the results of the dilution experiments which indicated a reduced stability against the dissociation of the fibrillar assemblies of mutProIAPP as compared to ProIAPP and IAPP. Protofibrillar and other non-fibrillar species have been described to ex-

hibit different CR binding than fibrils [54–56]. Also, differences between the amyloidogenic properties, morphological features and the tinctorial properties of the protein assembly forms have been reported to be caused even by a single mutation in an amyloidogenic protein [55,57,58].

In agreement with the observed good solubility and low aggregational potencies, the Trx-tagged fusion proteins were completely non-amyloidogenic, suggesting that introduction of the tag had resulted in disruption of both the self-association and amyloidogenic potentials of ProIAPP and mutProIAPP. A similar effect has been described for fusion moieties linked to other amyloid polypeptides [50].

The high portion of unordered elements (50%) seen for ProIAPP suggested a high conformational flexibility of this protein. This finding and the observed stability to heat denaturation were reminiscent of the reported flexibility of certain other amyloidogenic proteins including α-synuclein [59,60] and gelsolin [61].

The observed absence of any effects of temperature on the conformation and amyloidogenicity of ProIAPP indicated that the presence of the pro-region may have resulted in enhanced conformational stability compared to IAPP which had previously been observed to aggregate into amyloid fibrils at higher temperatures [13]. Also, unlike for IAPP [13], no evidence for the existence or stabilization of a specific partly unfolded, amyloidogenic precursor population was obtained for ProIAPP. The pro-region has been suggested to be essential for and to assist in protein folding for several proteins [62]. It has been proposed that pro-sequences could act as direct catalysts of folding by increasing the rate of on-pathway folding, acting to significantly decrease the life-time of protein folding intermediates and to result in a significant suppression of off-pathway aggregation [62,63]. On the other hand, protein aggregation and amyloid formation has been shown to proceed via partially folded states [64] and *in vivo*-formed amyloid essentially consists of the mature (processed) protein sequences. Thus, it appeared reasonable to speculate that the pro-region of an amyloidogenic polypeptide could serve to protect the amyloidogenic peptide against fibrillogenesis.

For several amyloidogenic polypeptides including Aβ, prion protein, α-synuclein, and IAPP, it has been shown that fibril formation occurs via a conformational transition into β-sheet structures [13,65–67]. Our studies showed that ProIAPP and mutProIAPP are able to aggregate into typical fibrillar assemblies under strong amyloidogenic conditions [12,13,29]. Under such amyloid-promoting conditions, however, it is not possible to investigate early events of the self-assembly pathway of ProIAPP and compare them with the corresponding events previously observed to occur dur-

ing IAPP amyloidogenesis [13]. By contrast, under the low-concentration conditions that were used for the CD aging experiments a direct follow-up of these events became possible.

Consistent with our previous observations, aging of IAPP, also when performed under the conditions applied herein for ProIAPP, led to a time-dependent conformational transition into soluble  $\beta$ -sheets and amyloid [13]. By contrast, aging, self-association and fibril formation of ProIAPP, proceeded via a distinct conformational transition that was characterized by a dramatic absolute decrease of the negative CD of non-aggregated ProIAPP between 200 and 240 nm with a subsequent nearly complete disappearance of the CD signal. MutProIAPP behaved like ProIAPP. None of the spectra obtained during ProIAPP- or mutProIAPP-aging exhibited the characteristic features of a transition into  $\beta$ -sheet structures [39] and no differences were detected between the secondary structure contents of the spectra obtained during the aging process. However, as the effect of size and quaternary structural rearrangement of  $\beta$ -sheets on their far-UV CD signal is unknown and as suitable reference spectra for stacked and multimeric  $\beta$ -sheet structures as found in an amyloid fibril are not yet available [39], the results of the visual or deconvolution-based predictions of secondary structure contents of amyloid-forming polypeptides should be interpreted with caution. The observed decrease in magnitude of the CD signal may have been due to a gradual increase in the corresponding positive CD signal in this region. Such a change of CD signal could occur during an ordered protein oligo- and multimerization process which is what occurs during aging, aggregation and fibril formation. In fact, dramatic effects of ordered self-association on the CD of non-aggregated compounds are known [68–70].

Our EM studies indicated that the species derived by the end of the conformational transition of ProIAPP under ‘diluted’ CD conditions consisted of both ordered but non-fibrillar species as well as of fibrils [10,11,42]. The morphological features of the non-fibrillar, ordered aggregates were very similar to recently described oligo- and multimeric structures of other proteins [10,43,44,65], confirming previous suggestions that there might be a common amyloid formation pathway [71].

The ProIAPP fibrillar assemblies that formed during the CD incubations associated laterally into broad sheet-like assemblies that were reminiscent of the assemblies that have been previously described for IAPP, A $\beta$ , and synuclein [10,43,65]. Of note, we did not detect the typical amyloid fibrillar bundles in the CD solution which had formed a predominant species when ProIAPP was incubated under fibrillogenic conditions. Laterally associated fibrillar assemblies were also the main species present, when solutions predominantly containing fibrillar ProIAPP

bundles were diluted up to 100  $\mu$ M, suggesting that they might be more stable against dissociation than typical fibrillar bundles. Polymorphism has been described in assemblies of IAPP solutions [10]. However, the morphological features of fibrillar assemblies have also been found to strongly depend on factors such as concentration, buffer, pH of the solution, properties of the assembly surface, etc. [43,56,72]. Thus, more studies will be necessary to determine if there is a relationship between typically observed ProIAPP fibrillar bundles and the laterally associated fibrils.

Unlike for ProIAPP, substantial amounts of typical fibrillar bundles were consistently present in CD solutions of aged IAPP solutions subsequent to the conformational transition into  $\beta$ -sheets. Importantly, these assemblies were also present after a 1000-fold dilution of IAPP fibrillar assemblies formed under fibrillogenic conditions (final IAPP concentration of 1  $\mu$ M), suggesting that they exhibited a markedly higher stability against dissociation than ProIAPP fibrils.

It should be stressed that the fibrillar assemblies identified following aging in the CD solutions corresponded to species formed by aging of the proteins from a denaturated and disaggregated state (8 M urea), i.e. at the beginning of this process. Therefore, identification of such species offers some information about the kinetic solubilities of the fibrillar assemblies [17]. By contrast, the species found following dilution of aged fibrillar solutions corresponded to species whose formation may be related to the dilution-driven dissociation of the fibrils. Studies on these species offer information about the stabilities of the fibrils against dissociation.

Together, the EM studies suggested: (1) that ProIAPP has a lower potential than IAPP to aggregate into typical amyloid fibrillar assemblies although it has a strong potential to aggregate into ordered oligomeric structures and (2) that ProIAPP fibrils are less stable against dissociation than IAPP fibrils. The large amounts of amorphous aggregates seen in the aged CD solutions of mutProIAPP together with our failure to detect fibrillar species in diluted fibrillar assemblies of mutProIAPP argue: (1) that mutProIAPP has a strong aggregational propensity to form amorphous aggregates that could be related to its high hydrophobicity and (2) that mutProIAPP fibrils have higher kinetic solubility and lower stability against dissociation than ProIAPP. These results would thus suggest the following order of amyloidogenicities: IAPP > ProIAPP  $\gg$  mutProIAPP.

A causal direct relationship between amyloid per se and cell death has yet to be shown. Nevertheless, aged solutions of various amyloidogenic sequences including IAPP have been found to be cytotoxic to a variety of cell types [6,7,22,73,74]. In this study, no cytotoxicity was found for the fusion proteins, a finding that was consistent with the

observed lack of amyloidogenicity of these proteins. By contrast, aged IAPP and ProIAPP solutions were cytotoxic, with ProIAPP being less toxic than IAPP. No cytotoxic properties were found for mutProIAPP. Of note, both the observed diminished cytotoxicity and lack of birefringence of recombinant mutProIAPP were confirmed by testing synthetic mutProIAPP prepared by SPSS methods (to be published in detail elsewhere).

The morphological features of the species responsible for amyloid-mediated cell toxicity are not yet defined [56,75]. In particular, there have been indications that both fibrillar and non-fibrillar ordered assemblies of amyloid peptides can cause cytotoxicity [6,74,76]. At the same time, there is evidence that amorphous aggregates of amyloidogenic peptides are not cytotoxic [74]. The lower cytotoxicities and amyloidogenicities found for ProIAPP and mutProIAPP as compared to IAPP would indicate that it is the fibrillar assembly form of these proteins that mediates cytotoxicity. However, our diluted *in vitro* incubation conditions were not identical to the *in situ* incubation conditions as performed for the cellular assays, as the latter also potentially involve cell medium-related effects and phenomena related to a direct protein–cell contact that may significantly affect the equilibria of fibril formation and dissolution. Such cell assay-like conditions cannot presently be simulated *in vitro*. In addition, the altered amyloidogenicity of mutProIAPP as compared to that of ProIAPP currently precludes conclusions with regard to the question of a need for proteolytic processing of ProIAPP to IAPP for cytotoxicity to occur. More detailed studies are necessary to address this issue.

The current lack of data of *in vivo* detectable ProIAPP-derived amyloid could be consistent with our findings. The high self-assembly potential of ProIAPP in combination with its lower amyloidogenicity as compared to that of IAPP could result in intracellular storage of the highly amyloidogenic IAPP in the form of non-fibrillar ProIAPP aggregates, thus ‘protecting’ the cell from ‘unwanted’ formation of pancreatic amyloid.

## Significance

IAPP is the major constituent of pancreatic amyloid in type II diabetes. It has been shown *in vitro* to exhibit a strong amyloidogenic and cytotoxic potential. *In vivo*, IAPP is stored as ProIAPP in secretory granules and secreted upon processing in response to insulin secretagogues. The aim of this study was to evaluate the conformational, biophysical and potentially amyloidogenic properties of ProIAPP, and to compare them to the properties of IAPP. To date, no method has been reported for the synthesis of ProIAPP. We devised an efficient method for the recombinant generation and purification of ProIAPP via a non-amyloidogenic Trx-His-tagged fusion protein. Under amyloid-promoting conditions, ProIAPP was found to be capable of

aggregating into typical amyloid fibrils. Furthermore, a strong self-associating potential was observed for ProIAPP which even aggregated at low micromolar concentrations. Nevertheless, ProIAPP was found to be markedly less amyloidogenic than IAPP. While aging of IAPP and other known amyloidogenic polypeptides occurs via aggregated  $\beta$ -sheets into typical amyloid fibrils, aging of ProIAPP was shown to occur by a distinct conformational transition which led to mixtures of fibrils with substantial amounts of non-fibrillar, yet ordered, oligo- and multimeric aggregates, suggesting that the process of ProIAPP aggregation and amyloidogenesis is distinguishable from the usually observed random coil-to- $\beta$ -sheet transition. Moreover, aged ProIAPP aggregates were less cytotoxic than those of IAPP. Cellular storage of proteins including IAPP secreted by the ‘regulatory’ pathway is usually achieved in their aggregated or ‘condensed’ forms. Thus, our studies would argue for a ‘protective’ role of the pro-region of ProIAPP against the high amyloidogenic and cytotoxic properties of IAPP. Protection could be conferred mechanistically by the ability of ProIAPP to self-assemble into ordered but non-fibrillar aggregates.

## Materials and methods

### Materials

Synthetic human IAPP was obtained from Calbiochem-Novabiochem (Bad Soden, Germany). Expression plasmids and host bacteria, His-Tag resin and recombinant Ek were from Novagen (Madison, WI, USA). Oligonucleotide primers were acquired from Life Technologies/Gibco BRL (Eggenstein, Germany). Rabbit polyclonal anti-IAPP antibody was from Peninsula Laboratories Europe (Merseyside, UK). Other molecular biology reagents, cell culture reagents and miscellaneous chemicals and enzymes were bought from Perkin Elmer-Applied Biosystems (ABI; Weiterstadt, Germany), Novagen, New England Biolabs (Heidelberg, Germany), or Sigma-Aldrich Chemicals (Deisenhofen, Germany) and were of the highest grade commercially available.

### Cloning of ProIAPP, mutProIAPP and fusion proteins

Human ProIAPP cDNA was prepared from peripheral blood mononuclear cells (PBMC) using standard procedures. Briefly,  $2.65 \times 10^7$  PBMC were isolated by Ficoll gradient centrifugation and total RNA isolated without further treatment of cells. PreProIAPP cDNA corresponding to a 270-bp sequence was then amplified by reverse transcription/polymerase chain reaction (RT/PCR) from 1  $\mu$ g RNA employing 35 amplification cycles (95°C for 45 s, 50°C for 1 min, 72°C for 45 s). Primers corresponding to the 5' and 3' ends of the human preProIAPP sequence were 5'-ATG GGC ATC CTG AAG CTG CAA GTA T-3' and 5'-CTA AAG GGG CAA GTA ATT CAG TGG C-3'. For cloning purposes, the proIAPP sequence was amplified from the preProIAPP cDNA template with the primers 5'-GAG ACC ATG GCT CCC ATT GAA AGT CAT CAG GTG GAA-3' and 5'-GAG AGC TCA GCC TAA AGG GGC AAG TAA TTC AGT GG-3'. Primers encompassed the *Nco*I and *B*l

I cloning sites, respectively, for insertion into the pET19b expression vector. PCR conditions for this step were as follows: 30 cycles at 94°C for 45 s, 55°C for 45 s, and 72°C for 30 s. The resulting 159-bp PCR product was then cloned into pET19b. For construction of the proIAPP–Trx fusion protein (Trx–ProIAPP), the pET32-LIC-vector system for ligation-independent cloning (LIC) was used. For amplification of this construct, primers 5'-GAC GAC GAC AAG ATC ACA CCC ATT GAA AGT CAT CAG GTG GA-3' and 5'-GAG GAG AAG CCC GGT CTA AAG GGG CAA GTA ATT CAG TGG-3' were applied and the PCR performed using the above protocol. The PCR product was cloned into the pET32-LIC vector

according to the manufacturer's recommendations. MutProlAPP DNA was generated by chemical oligonucleotide synthesis of three overlapping primers in combination with two successive PCR reactions. Primers were designed to span a DNA fragment corresponding to the ProlAPP cDNA sequence. Primer A included the *NcoI* cloning site and the N-terminal cleavage site mutation and primer C included the *BspI* cloning site and the C-terminal cleavage site mutation. In the first PCR reaction (35 cycles; 94°C for 45 s, 38°C for 1 min, 72°C for 30 s), primers A and B were annealed to yield a 5' fragment of 159-bp length containing the first mutation, i.e. that with the cleavage site between the N-terminal pro-sequence and IAPP changed. In a second PCR (35 cycles; 94°C for 45 s, 35°C for 1 min, and 72°C for 30 s), the obtained 159-bp fragment was annealed with primer C and the desired doubly mutated 224-bp product was amplified. Primer A was: 5'-CAT GCC ATG GCG CCC ATT GAA AGT CAT CAG GTG GAA **GCG GCG** AAA TGC AAC ACT GCC ACA TGT GCA ACG CAG CGC CTG GCA AAT TTT-3'; primer B was: 5'-**CGC** GCC ATA TGT ATT GGA TCC CAC GTT GGT AGA TGA GAG AAT GGC ACC AAA GTT GTT GCT GGA ATG AAC TAA AAA ATT TGC CAG GCG C-3'; and primer C was: 5'-AGA CGC TCA GCC TAA AGG GGC AAG TAA TTC AGT GGC TCT CTC TTT AAA ACC TCT ACT GCA TTC **GCC GCG** CCA TAT GTA TTG-3'. Mutated bases are shown bold and italic. The mutated PCR product was cloned into pET19b and the pET32-LIC vector as described above for wtProlAPP. All cloned DNA sequences were confirmed by bi-directional sequencing of at least two independent clones.

#### *Bacterial expression, purification and characterization of the fusion proteins*

Overexpression of the generated recombinant proteins was performed in *E. coli* BL21(DE3)pLys and was induced by IPTG for 3 h. Bacteria were harvested by centrifugation and cell pellets stored at -80°C. Immediately prior to purification, cells were thawed and disrupted by a French Press (1240 psi). As the recombinant proteins formed inclusion bodies, proteins needed to be solubilized. Various reagents including different chaotropic agents and detergents were tried. Insoluble protein was best solubilized by incubation in 20 mM TrisCl buffer, pH 7.9, containing 6 M urea for 2 h at RT. The use of GdnHCl, while equally efficient at the solubilization step, had adverse effects during the subsequent purification and renaturation steps (see below).

The His-Tag-containing fusion proteins Trx-ProlAPP and Trx-mutProlAPP were first purified by Ni<sup>2+</sup>-chelate affinity chromatography following the manufacturer's protocol. All buffers were adjusted to additionally contain 6 M urea. The obtained eluate was further purified by RP-HPLC. The following gradient program was applied for all RP-HPLC purifications performed in this study: step 1: 1 min at 10% buffer B in buffer A; step 2: 30 min from 10 to 90% buffer B in buffer A, with buffer A: 0.058% trifluoroacetic acid (TFA) in H<sub>2</sub>O and B: 90% acetonitrile, 0.05% TFA in H<sub>2</sub>O. The HPLC profiles of Figures 2D and 3D were obtained with the above gradient except that step 1 was 2 min in 10% buffer B in buffer A. The flow rate was 2 ml/min and detection was at 220 nm. A C<sub>18</sub>-column (Nucleosil 100 C18, dimensions: 250×8 mm, particle size 7 μm and pore size 100 Å) (Grom, Herrenberg, Germany) was used for all protein purifications. The fusion protein fractions were isolated, lyophilized and kept at -20°C. Identity of the fusion proteins was confirmed by SDS-PAGE (18 or 20% homogeneous gels) using a previously described method [12] and MALDI-MS or MALDI-TOF-MS using a Kratos Compact MALDI III machine (Shimadzu, Duisburg, Germany) or a G2025A LD-TOF-System Mass spectrometer (Hewlett Packard, Böblingen, Germany). In addition, immunoblotting analysis with an anti-IAPP antibody was performed as described [12], showing that both fusion proteins were detected by the IAPP-specific antibody.

#### *Cleavage of fusion tags, purification and characterization of ProlAPP and mutProlAPP*

Purified lyophilized fusion proteins were dissolved in a small volume of

10% acetic acid, neutralized with 10% NH<sub>4</sub>OH, and diluted with Ek reaction buffer (Novagen) to a final protein concentration of about 600 μg/ml. Eight U/ml of Ek were added and the reaction incubated at RT for 16–20 h. The resulting digests were lyophilized and kept at -20°C until purification. For purification of ProlAPP and mutProlAPP, digests were dissolved in 10% acetic acid and subjected to RP-HPLC as described above. Protein-containing fractions were lyophilized immediately and stored at -20°C. Purity grade and identity were verified by SDS-PAGE, HPLC and MS as described above.

#### *In vitro fibrillation and biophysical methods for fibril detection*

In vitro fibrillation of proteins was performed using a 2 mM protein solution in 10% acetic acid essentially as described [12,13]. Briefly, proteins were incubated for 4 days at RT, solutions neutralized with 10% NH<sub>4</sub>OH yielding a 1 mM working solution. The presence of amyloid was then verified by CR staining and EM.

The CR staining method for the detection of amyloid fibrils has been described [13]. Briefly, fibrillated protein solutions were allowed to air-dry on a glass microscope slide. Staining was performed by the addition of a saturated CR solution in 80% ethanol. Birefringence was determined with an Olympus CK40 light microscope (Olympus, Tokyo, Japan) under polarized light. For EM, 5–10 μl samples of the protein solutions or suspensions were applied on carbon-coated copper grids, stained with uranyl acetate and analyzed as described previously [13] using a Zeiss EM 109 electron microscope operated at 80 kV.

#### *CD spectropolarimetry*

CD spectra were recorded in a J-720 spectropolarimeter (Jasco, Tokyo, Japan). Cylindrical temperature-controlled quartz cells with a path length of 10 mm were used in all experiments. CD spectra were recorded at 25°C in the range between 200 and 300 nm at 0.2 nm intervals with a bandwidth of 1 nm, a scan speed of 50 nm/min, and a time constant of 8.0 s. Protein stock solutions were 500 μM in 10 mM sodium phosphate buffer, pH 7.4, containing 8 M urea and were usually kept at -20°C. Under these conditions, denaturated ProlAPP, mutProlAPP, and the fusion proteins were found to be soluble for several months. IAPP stocks in 8 M urea were prepared from a 500 μM IAPP stock in HFIP (kept at 4°C) [13] using the following procedure: an aliquot of the stock in HFIP was transferred into an Eppendorf tube and HFIP-evaporated at RT. To the pellet, an appropriate volume of 8 M urea in 10 mM sodium phosphate, pH 7.4 was added to obtain a 500 μM stock in 8 M urea which was then placed on ice and used immediately for the CD measurements. For CD measurements, protein stocks that had previously been thawed on ice, were directly diluted into a buffer-containing cuvette at RT (except for the IAPP stock which was diluted into the buffer at 4°C [13]) to give a final concentration of 5 μM protein (1 μM for the fusion proteins) in 10 mM sodium phosphate buffer, pH 7.4, containing 0.08 M urea and spectra were measured immediately or at various time points thereafter. Temperature denaturation studies were performed at a temperature increase rate of 2°C per min for up to 95°C as described [13]. Thereafter, temperature was decreased at the same rate down to 25°C. For aging studies, CD spectra were measured at various time intervals for up to 4–6 days following solution preparation at RT. Thereafter, solutions of ProlAPP and mutProlAPP were centrifuged (5 min at 17900×g) and 5–10 μl phosphate buffer (10 mM sodium phosphate, pH 7.4) was added to the pellets. Following mixing, solutions were added onto the EM grid, negatively stained and examined.

CD spectra are presented as a plot of the mean residue ellipticity ( $[\theta]$ , deg cm<sup>2</sup> dmol<sup>-1</sup>) versus the wavelength and represent net spectra, with the spectra of the buffer solution subtracted. CD spectra corresponding to non-time-dependent measurements represent the average of three measurements, while spectra corresponding to time-dependent measurements are from one measurement. The CD spectra shown in Figure 6 are representative of two to eight independently performed CD aging experiments.

### *In vitro* cytotoxicity studies

The rat insulinoma cell line RIN5fm was obtained from T.E. Rucinsky from the Washington University Tissue Culture Support Center and was cultured in RPMI 1640 containing 10% heat-inactivated fetal bovine serum, 2 mM L-glutamine, 0.1 mM non-essential amino acids, 1 mg/ml glucose, 1 mM sodium pyruvate and 0.1 mg/ml penicillin/streptomycin. Cells were plated in 96-well plates at a density of  $5 \times 10^5$  cells/ml (100  $\mu$ l/well). Following incubation for 24 h (37°C, humidified atmosphere with 5% CO<sub>2</sub>), serial dilutions of the aged IAPP, ProlAPP and mutProlAPP solutions consisting predominantly of fibrillar aggregates (made with 2 mM protein in 10% HAC; incubation time 4 days as described above) were made in cell culture medium and 11  $\mu$ l added into each well. Incubations were performed for 20 h and cell viability assessed by measuring the cellular reduction of 3-[4,5-dimethylthiazol-2-yl]-2,5-diphenyltetrazolium bromide (MTT) [12].

### Acknowledgements

We are grateful to G. Geiger for assistance with the expression of ProlAPP and mutProlAPP. We thank A. Kazantzis and A. Buck for HPLC purifications and the SPPS of mutProlAPP. We thank G. Tovar, S. Stoeva, M. Klärer, and K. Laib for MS measurements. We thank M. Duzsenko and G. Dußling for assistance with the EM. This work was supported by a grant from The University of Tübingen to A.K. and an institutional grant from the Fraunhofer IGB to J.B.

### References

- Westermarck, P., Wernstedt, C., Wilander, E., Hayden, D.W., O'Brien, T.D. & Johnson, K.H. (1987). Amyloid fibrils in human insulinoma and islets of Langerhans of the diabetic cat are derived from a neuropeptide-like protein also present in normal islet cells. *Proc. Natl. Acad. Sci. USA* **84**, 3881–3885.
- Clark, A., et al., & Turner, R.C. (1987). Islet amyloid formed from diabetes-associated peptide may be pathogenic in type II diabetes. *Lancet* **ii**, 231–234.
- Luskey, K.L. (1992). Possible links between amylin and diabetes. *Diabetes Care* **41**, 297–299.
- Cooper, G.J.S., Willis, A.C., Clark, A., Turner, R.C., Sim, R.B. & Reid, K.B.M. (1987). Purification and characterization of a peptide from amyloid-rich pancreases of type 2 diabetic patients. *Proc. Natl. Acad. Sci. USA* **84**, 8628–8632.
- Rink, T.J., Beaumont, K., Koda, J. & Young, A. (1993). Structure and biology of amylin. *Trends Pharmacol. Sci.* **14**, 113–118.
- Lorenzo, A., Razzboni, B., Weir, G.C. & Yankner, B.A. (1994). Pancreatic islet cell toxicity of amylin associated with type-2 diabetes mellitus. *Nature* **368**, 756–760.
- May, P.C., Boggs, L.N. & Fuson, K. (1993). Neurotoxicity of human amylin to rat primary hippocampal cultures: Similarity to Alzheimer's disease amyloid  $\beta$ -neurotoxicity. *J. Neurochem.* **61**, 2330–2333.
- Chargé, S.B.P., de Koning, E.J.P. & Clark, A. (1995). Effect of pH and insulin on fibrillogenesis of islet amyloid in vitro. *Biochemistry* **34**, 14588–14593.
- Cort, J., et al., & Anderson, N.H. (1994).  $\beta$ -Structure in human amylin and two designer  $\beta$ -peptides: CD and NMR spectroscopic comparisons suggest soluble  $\beta$ -oligomers and the absence of significant populations of  $\beta$ -strand dimers. *Biochem. Biophys. Res. Commun.* **204**, 1088–1095.
- Goldsbury, C.S., et al., & Kistler, J. (1997). Polymorphic fibrillar assembly of human amylin. *J. Struct. Biol.* **119**, 12–27.
- Goldsbury, C., Kistler, J., Aebi, U., Arvinte, T. & Cooper, G.J.S. (1999). Watching amyloid fibrils grow by time-lapse atomic force microscopy. *J. Mol. Biol.* **285**, 33–39.
- Kapurniotu, A., Bernhagen, J., Greenfield, N., Al-Abed, Y., Teichberg, S., Frank, R.W., Voelter, W. & Bucala, R. (1998). Contribution of advanced glycosylation to the amyloidogenicity of islet amyloid polypeptide. *Eur. J. Biochem.* **251**, 208–216.
- Kayed, R., Bernhagen, J., Greenfield, N., Sweimeh, K., Brunner, H., Voelter, W. & Kapurniotu, A. (1999). Conformational transitions of islet amyloid polypeptide (IAPP) in amyloid formation in vitro. *J. Mol. Biol.* **287**, 781–796.
- Ashburn, T.T. & Lansbury Jr., P.T. (1993). Interspecies variations affect the kinetics and thermodynamics of amyloid plaque formation: peptide models of pancreatic amyloid. *J. Am. Chem. Soc.* **115**, 11012–11013.
- Nishi, M., Sanke, T., Nagamatsu, S., Bell, G.I. & Steiner, D.F. (1990). Islet amyloid polypeptide: a new  $\beta$ -cell secretory product related to islet amyloid deposits. *J. Biol. Chem.* **265**, 4173–4176.
- Badman, M.K., Shennan, K.I., Jermany, J.L., Docherty, K. & Clark, A. (1996). Processing of pro-islet amyloid polypeptide (proIAPP) by the prohormone convertase PC 2. *FEBS Lett.* **378**, 227–231.
- Jarrett, J.T. & Lansbury Jr., P.T. (1993). Seeding one-dimensional crystallization of amyloid: a pathogenic mechanism in Alzheimer's disease and scrapie? *Cell* **73**, 1055–1058.
- Döbeli, H., et al., & Zulauf, M. (1995). A biotechnological method provides access to aggregation competent monomeric Alzheimer's 1–42 residue amyloid peptide. *Biotechnology (NY)* **13**, 988–993.
- Quibell, M., Turnell, W.G. & Johnson, T. (1995). Improved preparation of  $\beta$ -amyloid(1–43): structural insights leading to optimized positioning of *N*-(2-hydroxy-4-methoxybenzyl) (Hmb) backbone amide protection. *J. Chem. Soc. Perkin Trans. 1*, 2019–2024.
- Studier, F.W. (1991). Use of bacteriophage T7 lysozyme to improve an inducible T7 expression system. *J. Mol. Biol.* **219**, 37–44.
- Zhang, S., Liu, J., Saafi, E.L. & Cooper, G.J.S. (1999). Induction of apoptosis by human amylin in RINm5F islet  $\beta$ -cells is associated with enhanced expression of p23 and p21WAF1/CIP1. *FEBS Lett.* **455**, 315–320.
- Tenidis, K., et al., & Kapurniotu, A. (2000). Identification of a penta- and hexapeptide of islet amyloid polypeptide (IAPP) with amyloidogenic and cytotoxic properties. *J. Mol. Biol.* **295**, 1055–1071.
- Janciauskiene, S. & Ahren, B. (1998). Different sensitivity to the cytotoxic action of IAPP fibrils in two insulin-producing cell lines, HIT-T15 and RINm5F cells. *Biochem. Biophys. Res. Commun.* **251**, 888–893.
- Janson, J., Ashley, R.H., Harrison, D., McIntyre, S. & Butler, P.C. (1999). The mechanism of islet amyloid polypeptide toxicity is membrane disruption by intermediate-sized toxic amyloid particles. *Diabetes* **48**, 491–498.
- Mirzabekov, T.A., Lin, M. & Kagan, B.L. (1996). Pore formation by the cytotoxic islet amyloid peptide amylin. *J. Biol. Chem.* **271**, 1988–1992.
- Kyte, J. & Doolittle, R. (1982). A simple method of displaying the hydropathic character of a protein. *J. Mol. Biol.* **157**, 105–132.
- LaVallie, E.R., DiBlasio, E.A., Kovacic, S., Grant, K.L., Schendel, P.F. & McCoy, J.M. (1993). A thioredoxin gene fusion expression system that circumvents inclusion body formation in the *E. coli* cytoplasm. *Biotechnology (NY)* **11**, 187–193.
- Burdick, D., et al., & Glabe, C. (1992). Assembly and aggregation properties of synthetic Alzheimer's A4/ $\beta$  amyloid peptide analogs. *J. Biol. Chem.* **267**, 546–554.
- Westermarck, P., Engström, U., Johnson, K., Westermarck, G.T. & Betsholz, C. (1990). Islet amyloid polypeptide: pinpointing amino acid residues linked to amyloid fibril formation. *Proc. Natl. Acad. Sci. USA* **87**, 5036–5040.
- Cooper, J.H. (1974). Selective amyloid staining as a function of amyloid composition and structure. *Lab. Invest.* **31**, 232–238.
- Harper, J.D., Lieber, C.M. & Lansbury Jr., P.T. (1997). Atomic force microscopic imaging of seeded fibril formation and fibril branching by the Alzheimer's disease amyloid- $\beta$  protein. *Chem. Biol.* **4**, 951–959.
- Stine Jr., W.B., et al., & Krafft, G.A. (1996). The nanometer-scale structure of amyloid- $\beta$  visualized by atomic force microscopy. *J. Protein Chem.* **15**, 193–202.
- Wood, S.J., Maleeff, B., Hart, T. & Wetzel, R. (1996). Physical, morphological and functional differences between pH 5.8 and 7.4 aggregates of the Alzheimer's amyloid peptide A $\beta$ . *J. Mol. Biol.* **256**, 870–877.
- Harper, J.D. & Lansbury Jr., P.T. (1997). Models of amyloid seeding in Alzheimer's disease and scrapie: mechanistic truths and physiological consequences of the time-dependent solubility of amyloid proteins. *Annu. Rev. Biochem.* **66**, 385–407.
- Jaenicke, R. & Rudolph, R. (1989). Folding proteins. In: *Protein Structure. A Practical Approach* (Creighton, T.E., Ed.) pp. 191–223, IRL Press, Oxford.
- Perczel, A., Park, K. & Fasman, G.D. (1992). Analysis of the circular dichroism spectrum of proteins using the convex constraint algorithm: a practical guide. *Anal. Biochem.* **203**, 83–93.
- Brahms, S. & Brahms, J. (1980). Determination of protein secondary structure in solution by vacuum ultraviolet circular dichroism. *J. Mol. Biol.* **138**, 149–178.

38. Perczel, A., Park, K. & Fasman, G.D. (1992). Deconvolution of the circular dichroism spectra of proteins: the circular dichroism spectra of the antiparallel  $\beta$ -sheet in proteins. *Protein Struct. Funct. Genet.* **13**, 57–69.
39. Woody, R.W. (1985). Circular dichroism of peptides. In: *The Peptides, Analysis, Synthesis, Biology* (Udenfriend, S., Meienhofer, J., Hruby, V., Eds.) vol. 7, pp. 15–114, Academic Press, New York.
40. Wu, C.S. & Chen, G.C. (1989). Adsorption of proteins onto glass surfaces and its effect on the intensity of circular dichroism spectra. *Anal. Biochem.* **177**, 178–182.
41. Conway, K.A., Lee, S.-J., Rochet, J.-C., Ding, T.T., Williamson, R.E. & Lansbury Jr., P.T. (2000). Acceleration of oligomerization, not fibrillization, is a shared property of both  $\alpha$ -synuclein mutations linked to early-onset Parkinson's disease: implications for pathogenesis and therapy. *Proc. Natl. Acad. Sci. USA* **97**, 571–576.
42. Walsh, D.M., Lomankin, A., Benedek, G.B., Condron, M.M. & Teplow, D.B. (1997). Amyloid  $\beta$ -protein fibrillogenesis. Detection of a protofibrillar intermediate. *J. Biol. Chem.* **272**, 22364–22372.
43. Kowalewski, T. & Holtzman, D.M. (1999). In situ atomic force microscopy study of Alzheimer's  $\beta$ -amyloid peptide on different substrates: new insights into mechanism of  $\beta$ -sheet formation. *Proc. Natl. Acad. Sci. USA* **96**, 3688–3693.
44. Hatters, D.M., MacPhee, C.E., Lawrence, L.J., Sawyer, W.H. & Howlett, G.J. (2000). Human apolipoprotein C-II forms twisted amyloid ribbons and closed loops. *Biochemistry* **39**, 8276–8283.
45. Kuliopulos, A. & Walsh, C.T. (1994). Production, purification, and cleavage of tandem repeats of recombinant peptides. *J. Am. Chem. Soc.* **116**, 4599–4607.
46. Yansura, D.G. (1990). Expression as trpE fusion. *Methods Enzymol.* **165**, 161–166.
47. Lunn, C.A., Kathju, S., Wallace, B.J., Kushner, S.R. & Pigiet, V. (1984). Amplification and purification of plasmid-encoded thioredoxin from *Escherichia coli* K12. *J. Biol. Chem.* **259**, 10469–10474.
48. Schlumpberger, M., Wille, H., Baldwin, M.A., Butler, D.A., Herskowitz, I. & Prusiner, S.B. (2000). The prion domain of yeast Ure2p induces autocatalytic formation of amyloid fibers by a recombinant fusion protein. *Protein Sci.* **9**, 440–451.
49. Hollenbach, B., Scherzinger, E., Schweiger, K., Lurz, R., Lehrach, H. & Wanker, E.E. (1999). Aggregation of truncated GST-HD exon 1 fusion proteins containing normal range and expanded glutamine repeats. *Philos. Trans. R. Soc. Lond. B. Biol. Sci.* **354**, 991–994.
50. Scherzinger, E., et al., & Wanker, E.E. (1999). Self-assembly of polyglutamine-containing huntingtin fragments into amyloid-like fibrils: implications for Huntington's disease pathology. *Proc. Natl. Acad. Sci. USA* **96**, 4604–4609.
51. Litvinovich, S.V., Brew, S.A., Aota, S., Akiyama, S.K., Haudenschild, C. & Ingham, K.C. (1998). Formation of amyloid-like fibrils by self-association of a partially unfolded fibronectin type III module. *J. Mol. Biol.* **280**, 245–258.
52. Glover, J.R., Kowal, A.S., Schirmer, E.C., Patino, M.M., Liu, J.J. & Lindquist, S. (1997). Self-seeded fibers formed by Sup35, the protein determinant of [PSI<sup>+</sup>], a heritable prion-like factor of *S. cerevisiae*. *Cell* **89**, 811–819.
53. Lansbury Jr., P.T. (1992). In pursuit of the molecular structure of amyloid plaque: new technology provides unexpected and critical information. *Biochemistry* **31**, 6865–6870.
54. Walsh, D.M., et al., & Teplow, D.B. (1999). Amyloid  $\beta$ -protein fibrillogenesis. Structure and biological activity of protofibrillar intermediates. *J. Biol. Chem.* **274**, 25945–25952.
55. Lashuel, H.A., Wurth, C., Woo, L. & Kelly, J.W. (1999). The most pathogenic transthyretin variant, L55P, forms amyloid fibrils under acidic conditions and protofilaments under physiological conditions. *Biochemistry* **38**, 13560–13573.
56. Harper, J.D., Wong, S.S., Lieber, C.M. & Lansbury Jr., P.T. (1999). Assembly of A $\beta$  amyloid protofibrils: an in vitro model for a possible early event in Alzheimer's disease. *Biochemistry* **38**, 8972–8989.
57. McCutchen, S.L., Lai, Z., Miroy, G.J., Kelly, J.W. & Colon, W. (1995). Comparison of lethal and nonlethal transthyretin variants and their relationship to amyloid disease. *Biochemistry* **34**, 13527–13536.
58. Helms, L.R. & Wetzel, R. (1996). Specificity of abnormal assembly in immunoglobulin light chain deposition disease and amyloidosis. *J. Mol. Biol.* **257**, 77–86.
59. Weinreb, P.H., Zhen, W., Poon, A.W., Conway, K.A. & Lansbury Jr., P.T. (1996). NACP, a protein implicated in Alzheimer's disease and learning, is natively unfolded. *Biochemistry* **35**, 13709–13715.
60. Conway, K.A., Harper, J.D. & Lansbury Jr., P.T. (1998). Accelerated in vitro fibril formation by a mutant alpha-synuclein linked to early-onset Parkinson disease. *Nat. Med.* **4**, 1318–1320.
61. Ratnaswamy, G., Koepf, E., Bekele, H., Yin, H. & Kelly, J.W. (1998). The amyloidogenicity of gelsolin is controlled by proteolysis and pH. *Chem. Biol.* **6**, 293–304.
62. Eder, J. & Fersht, A.R. (1995). Pro-sequence-assisted protein folding. *Mol. Microbiol.* **16**, 609–614.
63. Agard, D.A. (1993). To fold or not to fold. *Science* **260**, 1903–1904.
64. Wetzel, R. (1996). For protein misassembly it's the 'I' decade. *Cell* **86**, 699–702.
65. Conway, K.A., Harper, J.D. & Lansbury Jr., P.T. (2000). Fibrils formed in vitro from  $\alpha$ -synuclein and two mutant forms linked to Parkinson's disease are typical amyloid. *Biochemistry* **39**, 2552–2563.
66. Pan, K.M., et al., & Cohen, F.E. (1993). Conversion of  $\alpha$ -helices into  $\beta$ -sheets features in the formation of the scrapie prion proteins. *Proc. Natl. Acad. Sci. USA* **90**, 10962–10966.
67. Soto, C. & Frangione, B. (1995). Two conformational states of amyloid  $\beta$ -peptide: implications for the pathogenesis of Alzheimer's disease. *Neurosci. Lett.* **186**, 115–118.
68. Nuckolls, C., Katz, T.J. & Castellanos, L. (1996). Aggregation of conjugated helical molecules. *J. Am. Chem. Soc.* **118**, 3767–3768.
69. Schnur, J.M., Ratna, B.R., Selinger, J.V., Singh, A., Jyothi, G. & Easwaran, K.R.K. (1994). Diacetylenic lipid tubules: experimental evidence for a chiral molecular architecture. *Science* **264**, 945–947.
70. Kim, M.-H., Ulibarri, L. & Keller, D. (1986). The psi-type circular dichroism of large molecular aggregates. III. Calculations. *J. Chem. Phys.* **84**, 2981–2989.
71. Rochet, J.-C. & Lansbury Jr., P.T. (2000). Amyloid fibrillogenesis: themes and variations. *Curr. Opin. Struct. Biol.* **10**, 60–68.
72. Lashuel, H.A., LaBrenz, S.R., Woo, L., Serpell, L.C. & Kelly, J.W. (2000). Protofilaments, filaments, ribbons, and fibrils from peptidomimetic self-assembly: implications for amyloid fibril formation and materials science. *J. Am. Chem. Soc.* **122**, 5262–5277.
73. Iversen, L.L., Mortishire-Smith, J., Pollack, S.J. & Shearman, M.S. (1995). The toxicity in vitro of  $\beta$ -amyloid protein. *Biochem. J.* **311**, 1–16.
74. Lorenzo, A. & Yankner, B.A. (1994).  $\beta$ -Amyloid neurotoxicity requires fibril formation and is inhibited by congo red. *Proc. Natl. Acad. Sci. USA* **91**, 12243–12247.
75. Lansbury Jr., P.T. (1999). Evolution of amyloid: what normal protein folding may tell us about fibrillogenesis and disease. *Proc. Natl. Acad. Sci. USA* **96**, 3342–3344.
76. Lambert, M.P., et al., & Klein, W.L. (1998). Diffusible, nonfibrillar ligands derived from A $\beta$ <sub>1–42</sub> are potent central nervous system neurotoxins. *Proc. Natl. Acad. Sci. USA* **95**, 6448–6453.